PBP1A and LdtJ support cell envelope homeostasis and impact selection of Colistin-resistance in *Acinetobacter baumannii*

Berenice Furlan[1,2], Sinjini Nandy[2#], Hanling Gong[2#], Michael B. Whalen[3], Nicolò Mattei[1], Roberto Jhonatan Olea-Ozuna[2], Daniela Vollmer[4], Waldemar Vollmer[4], Joseph M. Boll[2]*, and Orietta Massidda[1]*

Affiliations:

[1]Interdisciplinary Center for Medical Sciences (CISMed), Department of Cellular, Computational and Integrative Biology (CIBIO), University of Trento, Trento, Italy

[2]Department of Biological Sciences, University of Texas at Dallas, Dallas, USA

[3]Institute of Biophysics (IBF), National Research Council (CNR), Trento, Italy

[4]Institute for Molecular Bioscience, University of Queensland, Brisbane, Australia

[#]Authors contributed equally

*Correspondence:

Joseph M. Boll

The University of Texas at Dallas

Phone (972) 883-6529

Email: joseph.boll@utdallas.edu

Orietta Massidda

University of Trento

Phone +39 0461 283471

Email: orietta.massidda@unitn.it

Abstract

The multilayered cell envelope of *Acinetobacter baumannii* is an essential structure that maintains cellular integrity and protects the bacterial cell against external stresses and antibiotics. It consists of an inner membrane, a thin peptidoglycan (PG) layer and an asymmetric outer membrane (OM) enriched in lipooligosaccharide (LOS), whose lipid A moiety is the target of colistin, a last-resource antibiotic. Although lipid A is essential in most Gram-negatives, *A. baumannii* can survive without LOS through envelope remodeling, particularly in strains producing low levels of the bifunctional penicillin-binding protein PBP1A (encoded by *mrcA*) or in Δ*mrcA* mutants. Here, we identify a functional interplay between the LD-transpeptidase LdtJ, which generates 3-3 cross-links, and PBP1A, which catalyzes 4-3 transpeptidation during PG synthesis. We show that simultaneous inactivation of both enzymes severely affected growth, viability, morphology, and OM homeostasis. PG analyses revealed that the Δ*ldtJ* Δ*mrcA* mutants displays reduced overall cross-linkage and shorter glycan chains, producing a weakened sacculus. Co-immunoprecipitation demonstrated that PBP1A associates with LdtJ, supporting their coordinated activity at sites of PG synthesis. Notably, Δ*ldtJ* Δ*mrcA* mutants exhibited the highest recovery frequency of colistin-resistant, LOS-deficient variants compared with wild type or single mutants. Together, our findings demonstrate that coupling between 4-3 and 3-3 transpeptidation is critical for envelope stability in *A. baumannii* and highlight how disrupting this coordination favors the emergence of colistin resistance. This work identifies a conserved PG remodeling vulnerability that directly links PG integrity to the evolution of antibiotic resistance, offering a new conceptual framework for destabilizing the *A. baumannii* envelope.

46 **Importance**

47 The global rise of multidrug-resistant *Acinetobacter baumannii* represents an urgent clinical threat,
48 largely driven by its extraordinary capacity to withstand cell envelope damages and escape last-
49 resort antibiotics such as colistin. Although peptidoglycan synthesis and remodeling are known to
50 influence outer membrane stability, how these processes are coordinated in *A. baumannii* has
51 remained unclear. Here, we identify a crucial interplay between two critical envelope biogenesis
52 and remodeling activities, 4-3 and 3-3 transpeptidations, mediated by the bifunctional PBP1A and
53 the LD-transpeptidase LdtJ, respectively. Disrupting this coordination weakens the peptidoglycan,
54 destabilizes the outer membrane, and increases the emergence frequency of colistin-resistant,
55 LOS-deficient variants. These findings highlight a previously unrecognized vulnerability in the
56 envelope homeostasis of *A. baumannii*, suggesting that simultaneously targeting DD and LD-
57 transpeptidation could potentiate therapeutic strategies aimed at limiting antibiotic resistance
58 development.

59

60 **Keywords**

61 *Acinetobacter baumannii*, colistin resistance, lipooligosaccharide, penicillin-binding protein 1A,
62 LD-transpeptidase, peptidoglycan synthesis and remodeling, envelope integrity and homeostasis

63

64 **Introduction**

65 *Acinetobacter baumannii* is a Gram-negative opportunistic pathogen that has emerged as a major
66 concern in healthcare settings due to its remarkable capacity to survive environmental stress and
67 resist multiple classes of antibiotics (1), including last-resort agents such as colistin (2). This
68 resilience largely relies on the structural and functional integrity of the cell envelope, a
69 multilayered barrier essential for bacterial survival and defense against antimicrobial agents and
70 environmental challenges (3).

71 The Gram-negative cell envelope consists of three principal components: the inner
72 membrane (IM), the peptidoglycan (PG) layer, and the outer membrane (OM). The OM is
73 particularly notable for its asymmetric lipid organization: the inner leaflet consists of
74 phospholipids, whereas the outer leaflet is enriched with lipopolysaccharides (LPS), which
75 together form a highly selective permeability barrier (3,4). In *A. baumannii*, this role is fulfilled
76 by lipooligosaccharide (LOS), a truncated LPS variant lacking O-antigen polysaccharide (5).
77 Despite this structural difference, LOS is essential for OM stability and protects the bacterium
78 from toxic compounds and host immune factors.

79 Beneath the OM, the PG sacculus provides the cell with mechanical strength and osmotic
80 stability (6). PG consists of alternating *N*-acetylglucosamine and *N*-acetylmuramic acid that are
81 cross-linked by short peptides (7). In *Escherichia coli*, and many Gram-negative species, the
82 predominant 4-3 cross-links are formed by the DD-transpeptidase activity of penicillin-binding
83 proteins (PBPs), which link the fourth position D-alanine of a donor peptide to the third position
84 *meso*-diaminopimelic acid (*m*DAP) of an acceptor peptide (8). An alternative reaction, the
85 formation of 3-3 cross-links by LD-transpeptidases (LDTs), joins two *m*DAP residues and

86 typically increases under conditions that inhibit classical PG synthesis or impose envelope stress
87 (9–16).

88 In *A. baumannii*, 4-3 cross-links are similarly generated by PBPs, whereas the single LDT
89 in this species, LdtJ, catalyzes 3-3 cross-links that contribute to cell envelope robustness (9,17–
90 20). Although generally nonessential, LDTs are known to enhance resistance to β-lactam
91 antibiotics (10–13,17,21,22), protect against lysozyme (9), and support envelope integrity (19)
92 when OM assembly is impaired (15). LDT-mediated cross-linking often compensates for
93 perturbations in PG architecture to maintain envelope function (17). However, the extent to which
94 DD- and LD-transpeptidases coordinate PG synthesis and remodeling in *A. baumannii* remains
95 poorly understood.

96 To address this gap, we analyzed single and double mutants lacking *mrcA* or *mrcB*, which
97 encode class A PBPs PBP1A and PBP1B respectively, as well as *ldtJ*, in the multidrug-resistant
98 (MDR) clinical isolate AB5075. Loss of *mrcA* causes pronounced cell elongation, consistent with
99 a role for PBP1A in cell division (17,20), whereas deletion of *mrcB* produces minimal phenotypic
100 defects (17). Simultaneous deletion of *mrcA* and *mrcB* is synthetically lethal (17), underscoring
101 the essential and partially redundant functions. Previous work also proposed synthetic lethality
102 between *mrcA* and *ldtJ*, suggesting that LdtJ-mediated 3-3 cross-linking becomes indispensable
103 when PBP1A-dependent 4-3 cross-links are lost (17).

104 Here, we show that *ldtJ mrcA* double mutants are instead viable despite exhibiting severe
105 growth defects, pronounced morphological abnormalities, and compromised envelope
106 homeostasis. These phenotypes occur in both the clinical strain AB5075 and the laboratory strain
107 ATCC 17978, indicating that the functional interplay between PBP1A and LdtJ is crucial, albeit
108 not strictly essential, for *A. baumannii* cells.

109 We further examined how combined loss of *ldtJ* and *mrcA* influences the emergence of
110 colistin-resistant, LOS-deficient (ColR LOS$^-$) variants. Colistin exerts its bactericidal activity by
111 binding the phosphate groups of lipid A and displacing divalent cations, thereby disrupting OM
112 integrity (21,23). Although lipid A is essential in most Gram-negative bacteria, *A. baumannii* can
113 survive without it through inactivating mutations in *lpxA*, *lpxC*, and *lpxD*, which block LOS
114 biosynthesis (5,22). This LOS-deficient (LOS-) state imposes a substantial structural stress but can
115 be tolerated when *mrcA* function is reduced or absent (22), highlighting the critical
116 interdependence between PG and OM.
117 Collectively, our findings reveal that although *ldtJ* and *mrcA* are not synthetically lethal,
118 their combined inactivation disrupts growth, cell morphology, and envelope integrity. These
119 results uncover an underappreciated coordination between PG synthesis, maturation and
120 remodeling pathways and OM homeostasis in *A. baumannii*.
121

122 **Results**

123

124 **Deletion of *ldtJ* together with *mrcA*, but not with *mrcB*, impacts growth, viability and cell**

125 **morphology**

126 To investigate the functional interaction between LdtJ and PBP1A, we monitored growth of the *A.*

127 *baumannii* MDR strain AB5075 and mutants lacking either or both corresponding genes. The Δ*ldtJ*

128 Δ*mrcA* double mutant was generated in the Δ*ldtJ* background by removing first, *via* Cre

129 recombination, the Tn26 tetracycline resistance cassette, followed by transformation with genomic

130 DNA from the Δ*mrcA* mutant, as previously reported (24), and as detailed in the Materials and

131 Methods. Whole-genome sequencing verified the absence of suppressor mutations, as shown in

132 Fig. S1A and S1B. Likewise, a Δ*ldtJ* Δ*mrcB* double mutant was generated in strain AB5075 using

133 the same strategy.

134 Deletion of *ldtJ* or *mrcA* alone in AB5075 did not show a significant impact on growth

135 (Fig. 1A) or viability (Fig. 1B), in agreement with prior findings (17). In contrast, the Δ*ldtJ* Δ*mrcA*

136 double mutant, albeit viable, exhibited impaired growth relative to wild type and both single

137 mutants (Fig. 1A), coupled with a substantial reduction in viability (Fig. 1B). These findings

138 indicate a critical role for LdtJ and PBP1A in maintaining PG homeostasis.

139 Given these growth and viability defects, we next examined cell morphology. The Δ*ldtJ*

140 mutant displayed no appreciable differences compared to the wild type, whereas the Δ*mrcA* mutant

141 exhibited an elongated, chain-like phenotype with multiple or incomplete septa (Fig. 1C), in line

142 with the established role of *A. baumannii* PBP1A in cell division (17,20). The Δ*ldtJ* Δ*mrcA* double

143 mutant showed severe morphological abnormalities, producing markedly elongated cells than the

144 Δ*mrcA* single mutant (Fig. 1C). Quantitative measurements (n >100) confirmed that Δ*ldtJ* Δ*mrcA*

145 cells were significantly longer and narrower compared to the wild type and single mutants (Fig.
146 1D).

147 Consistent with the compromised LD-transpeptidase activity, both the Δ*ldtJ* single and the
148 Δ*ldtJ* Δ*mrcA* double mutant exhibited reduced incorporation of the fluorescent D-amino acid
149 analogue HADA relative to wild type, leading to a significant decrease in fluorescence intensity
150 (Fig. 1C and 1D). HADA is a non-canonical D-amino acid (NCDAA) predominantly incorporated
151 into *A. baumannii* by LdtJ, thus specifically labeling sites of active PG synthesis (17).

152 In contrast, the Δ*ldtJ* Δ*mrcB* double mutant resembled the wild type and the respective
153 single mutants with respect to growth and HADA incorporation, although these cells were
154 significantly thinner than wild type and the single mutants (Fig. S2).

155 Collectively, these results indicate that simultaneous deletion of *ldtJ* and *mrcA*, but not *ldtJ*
156 and *mrcB*, severely impacts the growth, viability, and morphology of *A. baumannii*. These data
157 also underscore that, despite the semi-redundancy and synthetic lethality between PBP1A and
158 PBP1B (17), the absence of PBP1A has a more profound impact for *A. baumannii*, particularly
159 when coupled with loss of LdtJ.

160 We examined the Δ*ldtJ* Δ*mrcA* phenotype also in the laboratory strain ATCC 17978. In
161 this background, deletion of *ldtJ* caused more pronounced defects than in AB5075, including a
162 mild growth delay and shape abnormalities characterized by shorter, rounder cells (Fig. S3A, S3B
163 and S3C; 17,19). As in AB5075, the ATCC 17978 Δ*mrcA* mutant displayed an elongated
164 phenotype (17), and the Δ*ldtJ* Δ*mrcA* double mutant exhibited elongated cells and exacerbated
165 morphological defects, (Fig. S3B and S3C).

166 Complementation analysis of the Δ*ldtJ* Δ*mrcA* double mutants with either *ldtJ* or *mrcA*
167 provided further insight. Ectopic expression of *ldtJ* (pLdtJ) in Δ*ldtJ* Δ*mrcA* double mutants

168 restored normal HADA incorporation but did not rescue cell shape in either AB5075 (Fig. S4A)
169 or ATCC 17978 (Fig. S4B). Conversely, expression of *mrcA* (pPBP1A) restored cell morphology
170 defects but did not restore HADA incorporation.
171
172 **Double inactivation of LdtJ and PBP1A also affects OM stability and integrity**
173 PG provides mechanical support to the bacterium to prevent lysis from the internal turgor. In
174 Gram-negative bacteria, the connection between PG and OM is an emerging theme (25). Although
175 LdtJ and PBP1A are enzymes involved in PG synthesis, maturation and remodeling, their function
176 may extend beyond PG assembly and editing, directly or indirectly. This relationship is grounded
177 in the fact that the PG meshwork and the OM form a coordinated structural unit (25), where
178 alterations in PG assembly can compromise OM anchoring and lipid organization, facilitating its
179 destabilization under stress conditions.
180 To explore this intimate connection, we assessed the susceptibility of the AB5075 *ldtJ* and
181 *mrcA* single and double mutants to agents challenging OM permeability, specifically rifampin (Fig
182 2A) at increasing concentrations and detergents, such as SDS or the combination of SDS and
183 EDTA (Fig 2B). The assays revealed that, whereas the individual loss of either enzyme resulted in
184 only small differences compared to the wild type, the simultaneous inactivation of *ldtJ* and *mrcA*
185 caused up to a four-log (10000-fold) reduction in growth in the presence of rifampin, SDS and
186 SDS/EDTA (Fig. 2A and 2B), suggesting increased OM permeability and loss of OM integrity.
187 To confirm that the observed phenotypes were directly caused by the loss of *ldtJ* and *mrcA*,
188 we used the AB5075 Δ*ldtJ* Δ*mrcA* double mutant expressing ectopically each gene individually
189 (Fig. S5). The Δ*ldtJ* Δ*mrcA* double mutant harboring the empty vector exhibited markedly reduced
190 growth in the presence of rifampin (0.562 μg/ml), whereas ectopic expression of either LdtJ or

191 PBP1A partially or completely restored the ability to grow in the presence of rifampicin,
192 respectively, rescuing the OM defects of the double mutant. These results reinforce the specific
193 and non-redundant contributions of both enzymes in maintaining OM stability and integrity in *A.*
194 *baumannii* and suggest that PBP1A plays a more prominent role than LdtJ in shaping PG structural
195 organization, as its expression more effectively restores growth under rifampin stress conditions.
196 Together, these findings not only demonstrate a direct role of LdtJ and PBP1A in PG
197 homeostasis but also highlight how PG maturation and remodeling critically influence OM
198 structure and function. The exacerbated permeability defects in the Δ*ldtJ* Δ*mrcA* double mutant
199 underscore the existence of parallel and partially redundant pathways that collaborate to uphold
200 the bacterial barrier, reinforcing the concept of an integrated functional network between the PG
201 and the OM in *A. baumannii*.
202
203 **Simultaneous inactivation of LdtJ and PBP1A redefines peptidoglycan architecture**
204 To investigate the physiological consequences of the simultaneous inhibition of the transpeptidase
205 activity of both LdtJ and PBP1A, we analyzed the PG composition of the AB5075 Δ*ldtJ* Δ*mrcA*
206 double mutant in comparison with the single mutants during both logarithmic and stationary phases
207 via HPLC and mass spectrometry (Fig. 3A and Fig. S6A).
208 In logarithmic phase, Δ*ldtJ* mutant showed a near-complete loss of 3-3 cross-links as
209 expected, confirming the pivotal role of LdtJ in catalyzing LD-transpeptidation also in the MDR
210 strain AB5075 (Fig. 3A and 3B; 17,19). The Δ*mrcA* mutant slightly increased 3-3 cross-links (Fig.
211 3B), suggesting higher activity of LdtJ in the absence of PBP1A. Interestingly, the mutants differed
212 in the levels of 4-3 cross-links in a similar way: as expected, the Δ*mrcA* mutant had decreased
213 levels of 4-3 cross-links whilst 4-3 cross-links were increased in the Δ*ldtJ* mutant, suggesting that

214 PBP1A activity was higher in the absence of LdtJ. Hence, cells appear to try compensating the
215 loss of LdtJ or PBP1A by enhancing the activity of the remaining transpeptidase, resulting in
216 altered contributions of 3-3 vs. 4-3 cross-links (Fig. S6B). Consistent with this, the double mutant
217 lacking both *ldtJ* and *mrcA* showed a significant reduced overall cross-linkage (Fig. 3B). Another
218 effect of the deletion of *ldtJ* was a strong reduction in tripeptides (Fig. 3A), presumably due to an
219 inherent LD-carboxypeptidase activity of LdtJ (19). In stationary phase, the effects on LD 3-3
220 cross-links and tripeptides of Δ*ldtJ* were also observed, but the differences in 3-3 and 4-3 cross-
221 links were less pronounced in all three mutants (Fig. S6 and Table S1). Anhydro-muropeptides
222 levels, indicative of glycan strand length, increased in the Δ*ldtJ* mutant and to a higher extent also
223 in the Δ*ldtJ* Δ*mrcA* double mutant in comparison to the wild type and the Δ*mrcA* mutant in
224 exponential phase, indicating a more fragmented PG network (Fig. 3C).

225 Together, these results demonstrate that LdtJ and PBP1A make nonredundant contributions
226 to overall PG composition and potentially compensate for the loss of the other in PG crosslinking
227 during exponential growth and stationary phase. Their combined absence produces a structurally
228 weakened sacculus, characterized by reduced 4-3 and 3-3 cross-links, and shorter glycan strands,
229 indicating a compromised PG robustness. These combined defects provide a molecular
230 explanation for the growth and viability impairment, altered morphology, increased OM
231 permeability, and overall envelope instability observed in the Δ*ldtJ* Δ*mrcA* double mutant, where
232 concurrent loss of LdtJ and PBP1A eliminates flexibility in PG synthesis, maturation and
233 remodeling.

234

235 **Co-IP reveals a direct interaction between PBP1A and LdtJ in *A. baumannii***

236 Given the functional interplay observed between PBP1A and LdtJ, we next tested whether these
237 proteins directly interact using co-immunoprecipitation (Co-IP). A C-terminal FLAG fusion
238 protein, LdtJ-FLAG was expressed in both the ATCC 17978 wild type and Δ*mrcA* mutant (Fig.
239 4). Immunoprecipitation of LdtJ-FLAG with an anti-FLAG resin followed by immunoblotting
240 revealed co-IP with PBP1A (Fig. 4), indicating that the two proteins associate *in vivo*, presumably
241 within the same complex. Importantly, no signal was detected in the LdtJ-FLAG pull-down with
242 the control protein RpoA, confirming interaction specificity. Immunoblots with the whole-cell
243 lysates were included as controls as detected by specific antibodies and Anti-FLAG antibody (Fig.
244 5A) To further validate this association, PBP1A-FLAG was also expressed in the wild type and
245 Δ*ldtJ* mutant (Fig 4) and subjected to Co-IP (Fig 4). LdtJ was consistently Co-IP'd with PBP1A-
246 FLAG, whereas non-specific proteins were absent. Together, these reciprocal Co-IP assays
247 provide evidence that PBP1A and LdtJ are part of the same protein complex *in vivo*.
248 The identification of this interaction provides a possible mechanistic explanation for the
249 synergistic phenotypes observed in the Δ*ldtJ* Δ*mrcA* double mutant. Since PBP1A synthesizes
250 classical 4-3 cross-linking and LdtJ catalyzes the alternative 3-3 linkages, their physical interaction
251 suggests that both enzymes may colocalize at sites of active PG assembly. Such spatial
252 coordination would enable a direct coupling, or alternatively competition, between 4-3 and 3-3
253 cross-linking activities, thereby optimizing PG robustness during growth and division under stress
254 conditions.
255
256 **Additive recovery of LOS-deficient, colistin-Resistant variants in the Δ*ldtJ* Δ*mrcA* mutant**
257 The ability to generate colistin-resistant variants through loss of LOS varies among *A. baumannii*
258 strains (17,22). While strains such as AB5075 and ATCC 19606 can naturally develop colistin

259 resistance, strain ATCC 17978 is dependent on LOS for viability unless mutations, such as *mrcA*
260 inactivation (17,22), are present to produce a permissive state. In this context, it is critical to
261 understand how the combined inactivation of *ldtJ* and *mrcA* influences the frequency and
262 phenotype of colistin-resistant variants in AB5075.

263 Determination of the LOS$^-$ recovery frequency revealed low frequency of ColR LOS$^-$
264 variants in the AB5075 wild type of 6.3×10^{-10}. Single Δ*ldtJ* and Δ*mrcA* mutants showed increased
265 recovery frequencies to 6.9×10^{-9} and 4.9×10^{-8}, respectively. The Δ*ldtJ* Δ*mrcA* double mutant,
266 moreover, exhibited the highest recovery frequency of 1.07×10^{-7}, reflecting an effect that
267 substantially promotes the selection of ColR LOS$^-$ variants (Fig. 5A). In contrast, the single Δ*mrcB*
268 mutant, and the Δ*ldtJ* Δ*mrcB* double mutant, failed to generate ColR LOS$^-$ variants under the tested
269 conditions (Fig. 5A). Similar experiments in the ATCC 17978 genetic background, where
270 spontaneous selection of ColR LOS$^-$ variants is inaccessible (22), showed no recovery of ColR
271 variants in the wild type or in the Δ*ldtJ* mutant, as previously shown (17,22). The Δ*mrcA* mutant
272 exhibited a frequency of 4.4×10^{-9} and the Δ*ldtJ* Δ*mrcA* double mutant showed a relative increase
273 in recovery frequency of 7.4×10^{-8}, supporting the conclusion that the combined inactivation of
274 *mrcA* and *ldtJ* favors the selection of ColR LOS$^-$ variants across different *A. baumannii* genetic
275 backgrounds.

276 To test the lack of LOS in the isolated ColR variants generated by the AB5075 Δ*ldtJ* Δ*mrcA*
277 mutant, proteinase K-treated cell lysates were analyzed for relative LOS levels by SDS-PAGE
278 analysis. The wild type, the Δ*ldtJ* and Δ*mrcA* single mutants exhibited comparable LOS levels, as
279 did the Δ*ldtJ* Δ*mrcA* parental strain (Fig. 5B). However, the Δ*ldtJ* Δ*mrcA* ColR variant lacked
280 detectable LOS, confirming a LOS- phenotype (Fig. 5B). Moreover, the AB5075 Δ*ldtJ* Δ*mrcA*
281 ColR LOS- variant displayed reduced viability (CFU/ml) on LB agar compared to the Δ*ldtJ* Δ*mrcA*

282 parental strain (Fig. 3C, upper panel), suggesting a fitness cost associated with LOS deficiency, as
283 has been reported with LOS- strains (26,27). Yet, in the presence of colistin (10 µg/ml), only Δ*ldtJ*
284 Δ*mrcA* ColR LOS⁻ variant grew while the Δ*ldtJ* Δ*mrcA* parental strain did not grow (Fig 3C,
285 middle panel). On the contrary, the presence of vancomycin (10 µg/ml) completely inhibited the
286 growth of the Δ*ldtJ* Δ*mrcA* ColR LOS⁻ variant but not of the parental strain, highlighting altered
287 OM permeability linked to LOS deficiency (Fig. 5C, bottom panel). The Minimum Inhibitory
288 Concentrations (MICs), determined by E-test, demonstrated that the Δ*ldtJ* Δ*mrcA* parental strain
289 was susceptible to colistin but resistant to vancomycin, bacitracin, and daptomycin, in line with
290 previous reports on LOS- *A. baumannii* strains (22,47). Conversely, the Δ*ldtJ* Δ*mrcA* ColR LOS-
291 variant was resistant to colistin but became susceptible to the other antibiotics (Fig. 5D),
292 presumably reflecting significant changes in OM permeability and consequent decreased MICs
293 associated with LOS deficiency.

294 Growth curve analyses (OD_{600}) corroborated these observations: the wild type and the
295 Δ*ldtJ* Δ*mrcA* ColS LOS+ parental strain grew well in LB broth but was inhibited by colistin,
296 whereas the ColR LOS- variant not only grew in the presence of colistin but also exhibited
297 enhanced growth rates compared to antibiotic-free conditions (Fig. 5E), suggesting an advantage
298 under colistin pressure. We further characterized the Δ*ldtJ* Δ*mrcA* ColR LOS- variants by
299 fluorescence microscopy using FM5-95 membrane staining. The Δ*ldtJ* Δ*mrcA* ColR LOS- variant
300 exhibited cell "clumping" and “ballooning” when grown in LB without colistin; these phenotypes
301 diminished notably upon exposure to colistin (Fig. 5F), which presumably stabilizes the remodeled
302 OM during antibiotic stress (26, 27).

303 Together, these data demonstrate that simultaneous inactivation of *ldtJ* and *mrcA* increases
304 the recovery frequency of ColR LOS- variants providing new insights into the compensatory
305 mechanisms that *A. baumannii* employ to survive antimicrobial stress.
306
307 **Discussion**
308 The coordination between PG synthesis and remodeling and OM integrity represents a
309 fundamental aspect of envelope homeostasis in Gram-negative bacteria. In *A. baumannii*, however,
310 this interplay is yet largely unexplored despite its critical role in antibiotic resistance (17,28,29)
311 and virulence (30,31).
312 Our results demonstrate that the LD-transpeptidase LdtJ and the septal bifunctional class
313 A PBP1A act in a coordinated manner to preserve envelope stability and integrity. Contrary to
314 previous hypotheses (17), the simultaneous inactivation of LdtJ and PBP1A is not lethal but
315 produces severe phenotypic and fitness defects. While the coordinated transpeptidation appears
316 conserved, strain dependent effects were also observed. Inactivation of LdtJ alone in AB5075 does
317 not induce obvious defects in cell growth, viability, or morphology (Fig. 1A and Fig. 1B), while
318 in the 17978 Δ*ldtJ* mutant morphology is perturbed (Fig. S3). However, in both strains Δ*ldtJ*
319 Δ*mrcA* double mutants showed severe defects characterized by reduced growth rate and viability,
320 elongated and multiseptated cells with incomplete septa, and compromised OM homeostasis. Our
321 PG analysis highlights that the 3-3 cross-linking formed by LdtJ and the 4-3 crosslinks synthetized
322 by PBP1A represent parallel PG biosynthetic, maturation and remodeling activities that ensure a
323 robust PG network and, together, confer the stability and the structural support to the cell envelope.
324 While the model organism *E. coli* has six LDTs, of which the LdtE generates most 3-3
325 cross-links in stationary phase (8,32) and LdtD becomes essential in complex with PBP1B and the

326 DD-carboxypeptidase PBP6a to support the PG structure when the transport of the LPS to the OM
327 is compromised (15), *A. baumannii* can only rely on LdtJ for the synthesis of the 3-3 cross-links.
328 *E. coli* LdtD has been proposed to work in concert with the PBP1B, the major class A PG synthase
329 involved in cell division, forming a "PG repairing" complex with PBP6a, which trims the
330 pentapeptides to increase the pool of tetrapeptides to form the 3-3 cross-links. This machinery
331 would reinforce the cell wall structure repairing the PG meshwork when the OM is compromised,
332 providing an important model to demonstrate the intimate connection between PG remodeling and
333 OM integrity (15). According to our data, it is reasonable to propose a model where LdtJ and
334 PBP1A act within the same functional complex to optimize PG synthesis, maturation and
335 remodeling. When one enzyme is inactivated, the other can partially compensate; however, the
336 simultaneous loss of both enzymes results in severe defects in PG structure and integrity.

337 In *E. coli*, PBP1A and PBP1B are semi-redundant enzymes that can compensate for each
338 other, and LDTs are generally dispensable under normal growth conditions (33,34). In contrast,
339 our results indicate that when LD-transpeptidation is lost in *A. baumannii*, PBP1B cannot
340 compensate for the loss of PBP1A. Furthermore, double inactivation of LdtJ and PBP1A, unlike
341 inactivation of LdtJ and PBP1B, severely compromises the envelope integrity. This divergence
342 suggests that, unlike *E. coli*, *A. baumannii* may have a reduced capacity to compensate for the loss
343 of key PG biosynthetic enzymes, likely due to the limited functional redundancy in its genome.

344 The effects of the double LdtJ and PBP1A inactivation emerged also from our PG analysis.
345 Consistent with LdtJ being the sole LDT in *A. baumannii* and with previous studies in the ATCC
346 17978 background (17,19), the Δ*ldtJ* mutant exhibited almost complete loss of 3-3 linkages and a
347 decreased pool of total tripeptides fraction in comparison to the wild type. However, no differences
348 in the incorporation of NCDAAs, other than D-Ala, were observed in the AB5075 Δ*ldtJ* mutant,

349 differently from what reported in the ATCC 17978 Δ*ldtJ* (17,19) and in other Gram-negative
350 bacteria like *E. coli* and *Vibrio cholerae* (35,36). This can be explained by the fact that also the
351 AB5075 wild type doesn't show incorporation of NCDAAs.

352 These strain-dependent differences between *A. baumannii* different genetic backgrounds
353 could possibly reflect variations in the pool of LdtJ tetrapeptides substrates or acceptors and may
354 provide an explanation for the different morphological phenotypes observed in the AB5075 Δ*ldtJ*
355 (wild type-like) and ATCC 17978 Δ*ldtJ* (rounder) mutants.

356 In contrast, the Δ*mrcA* mutant consistently accumulated 3-3 cross-links across both genetic
357 backgrounds compared to the wild type. This feature, interpreted as a possible requirement to
358 substitute the 4-3 cross-links with more 3-3 cross-links in the absence of PBP1A (17), can now be
359 more plausibly considered an indirect consequence of increased availability of tetrapeptide
360 substrates for LdtJ**,** rather than a direct compensatory mechanism to reinforce PG structure.
361 Strikingly, the Δ*ldtJ* Δ*mrcA* double mutant nearly abolished 3-3 links but also significantly reduced
362 overall cross-linkage, with a drop in the average glycan chain length, yielding a sacculus that is
363 less cross-linked and structurally weakened. These changes provide a direct molecular explanation
364 for the reported growth, viability, morphological defects, increased OM permeability and
365 instability observed in the Δ*ldtJ* Δ*mrcA* double mutant. In *E. coli*, LDTs, such as LdtD and LdtE,
366 are known to become particularly important under β-lactam-induced stress or in strains with
367 perturbed PG synthesis (13). Our results suggest that a similar stress-compensatory role for LD-
368 transpeptidation also exists in *A. baumannii*, but that its interplay with PBP1A is more critical for
369 maintaining basal envelope integrity.

370 The envelope defects in Δ*ldtJ* Δ*mrcA* extend to the OM permeability and integrity that was
371 probed by testing its susceptibility to the hydrophobic antibiotic rifampin and the detergent SDS

372 alone or combined with the chelator EDTA. The Δ*ldtJ* Δ*mrcA* double mutant showed a synergistic
373 increase in susceptibility to rifampin, and to detergent/chelator combinations (SDS and
374 SDS/EDTA), as it is more sensitive than the single mutants at all the probed concentrations and
375 conditions. These defects were rescued by ectopic expression of either *ldtJ* or *mrcA*. Because the
376 PG and OM form a mechanically coupled unit (37), a reduction in PG cross-linking likely impacts
377 the OM structure altering its permeability and integrity properties. We propose that the combined
378 loss of 3-3 cross-links and the reduced efficiency of 4-3 cross-linking disrupts the tension balance
379 across the envelope, lowering the threshold for OM failure under chemical stress.

380 We also show that PBP1A physically interacts with LdtJ *in vivo*. The immunoprecipitation
381 of PBP1A-FLAG recovered LdtJ, and the reciprocal co-IP of LdtJ-FLAG recovered PBP1A,
382 supporting the idea that these enzymes operate in the same molecular complex. Such direct
383 interaction may facilitate the spatial coordination of 4-3 and 3-3 cross-linking activities at the
384 septum, ensuring a robust PG synthesis and remodeling. In *E. coli*, LdtD has been shown to
385 physically interact with the class A septal PBP1B forming a complex in cells with OM assembly
386 defects by fortifying the sacculus and preventing cell lysis (15). Beyond its role in supporting the
387 cell envelope homeostasis, the association between LdtD and PBP1B and PBP5 has been proposed
388 to strategically localize LdtD and facilitate its access to PBP1B and PBP5 substrates, mediating in
389 this way β-lactam resistance (38).

390 Finally, a striking evolutionary consequence of disrupting this coordination was the
391 increased selection of ColR LOS- variants in the Δ*ldtJ* Δ*mrcA* mutant. These findings suggest that
392 the destabilization of the PG network can drive adaptive remodeling in the OM. In AB5075, the
393 recovery frequency of ColR LOS- increased from wild type to the single mutants and was highest
394 in the double mutant. A similar additive trend, though at lower absolute frequencies, was observed

395 in the ATCC 17978. The Δ*ldtJ* Δ*mrcA* ColR variants lacked detectable LOS by gel staining,
396 became susceptible to vancomycin and other antibiotics with poor OM penetration. The Δ*ldtJ*
397 Δ*mrcA* ColR LOS- variants also exhibited morphology abnormalities, which were exacerbated
398 when grown in drug-free conditions. Although slower growth rates and altered cell shape in *A.*
399 *baumannii* LOS- have been reported (39), the mechanism by which collapse of the PG-OM system
400 supports LOS deficiency while maintaining lipid bilayer integrity remains unclear. From a
401 therapeutic perspective, the fitness costs observed in the Δ*ldtJ* Δ*mrcA* ColR LOS- variants suggest
402 that the simultaneous inhibition of DD- and LD-transpeptidation combined with OM-
403 permeabilizing adjuvants could potentiate envelope destabilization. The LdtJ-PBP1A system may
404 therefore represent a druggable target in MDR *A. baumannii* clinical isolates.

405 Together, this work underscores that LdtJ and PBP1A form a functionally integrated
406 system that coordinates PG synthesis, maturation and remodeling with OM stability and integrity.
407 Balanced synthesis of 4-3 and 3-3 cross-links at the sites of active PG synthesis ensures mechanical
408 strength and flexibility of the sacculus, thus contributing to the preservation of OM barrier
409 function. Disruption of this equilibrium, however, paves the way for adaptive mechanisms that
410 allow the development of colistin resistance via loss of LOS.

411

412 **Material and Methods**

413 **Bacterial strains and growth conditions**

414 All bacterial strains and plasmids used in this study are listed in Table S2, and the oligonucleotides
415 are provided in Table S3. *A. baumannii* and *E. coli* were routinely grown aerobically on Luria-
416 Bertani agar or Lysogeny Broth (LB) at 37°C from frozen stocks preserved at 30% glycerol at -
417 80°C. For selection, antibiotics were added to the growth media, when necessary, at the following

418 final concentrations: tetracycline (5 µg/ml for AB5075 or 10 µg/ml for ATCC 17978) (40),
419 hygromycin (250 µg/ml for AB5075) (40), kanamycin (25 µg/ml), colistin (10 µg/m), and
420 vancomycin (10 µg/ml). Diaminopimelic acid (DAP) was added at 600 µM to support the growth
421 of *E. coli* DAP$^-$ donor strain. IPTG (isopropyl β-D-1-thiogalactopyranoside) was added at varying
422 concentrations to induce gene expression as indicated.
423
424 **Construction of AB5075 *A. baumannii* double mutants and ectopic expression of *ldtJ* and**
425 ***mrcA***
426 Isogenic mutants with transposon insertion were obtained from the *A. baumannii* AB5075 ordered
427 mutant library of the Laboratory of Colin Manoil (University of Washington) (40). The double
428 mutants Δ*ldtJ* Δ*mrcA* and Δ*ldtJ* Δ*mrcB* were generated by a two-steps protocol based on Cre
429 recombination followed by natural transformation of genomic DNA (40). Briefly, the tetracycline
430 resistant cassette of the recipient single mutant was removed by site-specific recombination.
431 Subsequently, purified genomic DNA of the donor mutant was mixed 1:1 with the recipient mutant
432 grown to early logarithmic phase (OD_{600} 0.2 – 0.3), spotted on freshly prepared LB agar and
433 incubated for 4 hours at 37°C. After incubation the bacteria were resuspended in PBS and spotted
434 on LB agar supplemented with tetracycline for selection and incubated at 28°C overnight.
435 Mutations were confirmed by PCR and verified by Whole Genome Sequencing (WGS). Two
436 independent double mutant isolates were characterized and only one is shown. The *ldtJ*
437 (ABUW_118) and *mrcA* (ABUW_0289) genes were cloned into the BamHI/XbaI restriction sites
438 of the replicative plasmid pJMP3665^{HygR} (41). pJMP3665*::ldtJ* was introduced into *E. coli* DAP$^-$
439 mating strain, and an overnight culture was mixed at equal ratios with an overnight culture of the
440 Δ*ldtJ* Δ*mrcA* recipient mutant for conjugative transfer. The cell mixture was spotted on an LB

441 plate supplemented with DAP and incubated at 37°C for 3 hours. After this, grown bacteria were
442 resuspended in PBS and spotted on LB agar supplemented with 250 µg/ml hygromycin for
443 selection and incubated at 37°C overnight (41). LdtJ expression was induced by adding 1 mM of
444 IPTG. pJMP3665*::mrcA* was introduced the Δ*ldtJ* Δ*mrcA* recipient mutant by electroporation of
445 the ligation product. Briefly, the recipient culture was grown at 37°C until mid-logarithmic phase
446 (OD_{600} ~0.4). After this, cells were washed five times with 10% ice-cold glycerol. 500 ng of
447 ligation DNA was electroporated into the recipient cells in a 2-mm cuvette at 1.8 kV. Cells were
448 recovered in LB broth in shaking conditions for 1 hour at 37 °C and plated on an LB agar plate
449 supplemented with 250 µg/ml hygromycin. PBP1A expression was induced by adding 10 µM
450 IPTG.
451
452 **Construction of ATCC 17978 Δ*ldtJ* Δ*mrcA* double mutant and ectopic expression of *ldtJ* and**
453 ***mrcA***
454 ATCC 17978 Δ*ldtJ* Δ*mrcA* double mutant was generated as previously described (17,29,42,43) by
455 introducing the recombinase plasmid $pMMB67EH^{TetR}$ encoding REC_{Ab} in the Δ*mrcA* single
456 mutant. Expression of the REC_{Ab} was induced by adding 2 mM IPTG and cells were grown at
457 37°C until mid-logarithmic phase (OD_{600} ~0.4-0.5). After washing with 10% ice-cold glycerol, the
458 linear PCR product targeting *ldtJ* with 125 bp region of homology and containing the kanamycin
459 resistance cassette FLP recombination target (FRT) was electroporated into this mutant. Cells were
460 recovered in LB broth in shaking conditions with 2 mM IPTG for 4 hours and plated on LB agar
461 supplemented with 25 µg/ml kanamycin for selection. The mutation was verified by PCR. Mutants
462 were then treated to remove the $pMMB67EH^{TetR}$*::*REC_{Ab} by restreaking on LB agar containing 2
463 mM $NiCl_2$ (29,42,43). Mutants that lost the tetracycline resistance cassette were then

464 electroporated with pMMB67EH^{TetR} carrying the FLP recombinase to excide the kanamycin
465 cassette after recovering for 1 hour in LB broth and plating on LB agar with 10 µg/ml tetracycline
466 and 2 mM IPTG to induce the expression of FLP. The kanamycin cassette excision was verified
467 by PCR.

468 To ectopically express the *ldtJ* (A1S_2371) and *mrcA* (A1S_3196-97) genes, pMMB*::ldtJ*
469 and pABBR*::mrcA* (with its native promoter) were electroporated in the of ATCC 17978
470 Δ*ldtJ*Δ*mrcA* double mutant to generate Δ*ldtJ*Δ*mrcA*/pLdtJ and Δ*ldtJ*Δ*mrcA*/pPBP1A strains,
471 respectively. The Δ*ldtJ*Δ*mrcA*/pLdtJ strain was selected with 25 µg/ml kanamycin and *ldtJ*
472 expression induced with 2 mM IPTG whereas the Δ*ldtJ*Δ*mrcA*/pPBP1A strain was selected with
473 10 µg/ml tetracycline and *mrcA* induction was constitutive.

474

475 **Growth curves and viability**

476 Overnight cultures of AB5075 were diluted 1:50 in 12.5 ml of LB broth and pre-cultured to early
477 logarithmic phase (OD_{600} 0.2-0.3) at 37°C with continuous shaking. At this point, pre-cultures
478 were back-diluted 1:50 in 50 ml of LB broth, incubated at 37°C with continuous shaking and the
479 growth was monitored by manually measuring the optical density at 600 nm every 30 minutes for
480 6 hours. Samples for viable counts were collected every 1.5 hours, serially diluted and plated on
481 LB agar. Plates were incubated overnight at 37°C and the colony forming units (CFUs) were
482 counted. Growth and viability were plotted using GraphPad Prism 10 (version 10.2.3). Each
483 experiment was independently performed three times, and representative datasets are shown.

484 Overnight cultures of strain ATCC 17978 were back-diluted to an initial OD_{600} of 0.01 and
485 inoculated into 5 ml of LB broth in triplicate. Cultures were incubated at 37°C with continuous
486 shaking. Optical density at 600 nm was manually measured every hour for 10 hours. Growth curves

487 were generated using GraphPad Prism 10 (version 10.2.3). Each experiment was independently
488 performed three times, and representative datasets are shown.
489
490 **Microscopy and image analysis**
491 Overnight cultures were diluted to an OD_{600} of 0.05 and grown in LB broth in shaking conditions
492 at 37°C until reaching an OD_{600} of ~0.4–0.5 (mid-logarithmic phase). The appropriate antibiotic
493 and IPTG were added to the grown strains. Cells were harvested and washed in LB before being
494 incubated with 10 mM HADA (7-hydroxycoumarincarbonylamino-D-alanine, Thermo Fisher
495 Scientific) in LB broth for 20 min at 37°C, with shaking in dark conditions, to fluorescently label
496 the sites of active peptidoglycan biosynthesis. After further washes, cells were resuspended in 1X
497 phosphate-buffered saline (PBS) and fixed with 16% paraformaldehyde (PFA) and mounted on
498 1.5% agarose in 1X PBS pads on microscopy slides. Imaging was performed using an inverted
499 Nikon Eclipse Ti-2 widefield epifluorescence microscope equipped with a Photometrics Prime
500 95B camera and a Plan Apo 100×, 1.45 NA objective lens. Images were acquired using NIS
501 Elements software, and image analysis was carried out using the MicrobeJ plugin in Fiji. Cell
502 length, width, aspect ratio, and fluorescence intensity were measured for at least 100 analyzed cells
503 per experiment and plotted in GraphPad Prism 10 (version 10.2.3).
504 For FM 5-95 staining, cell cultures were collected at mid-logarithmic phase (OD_{600} ~0.4),
505 harvested by centrifugation and resuspended in 100 µl of 5% PFA solution (Immunofix, Bio-
506 Optica). To stain and visualize membranes, cells were incubated with the FM 5-95 dye at a final
507 concentration of 5 µg/ml for 10 minutes at room temperature, washed twice in PBS and
508 resuspended in a 1:4 ratio of ProLong™ Gold antifading (Thermo Fisher Scientific) and visualized
509 at the microscope. Imaging was performed using an inverted Nikon Eclipse Ti2 equipped with a

510 CREST V3 X-light Spinning Disc confocal module, Lumencor CELESTA multi-line lasers, a
511 monochromatic sCMOS camera, and a monochromatic EMCCD camera for widefield and
512 spinning disc acquisitions. Images were captured with an exposure time of 80 ms and an emission
513 wavelength of 683 nm. For the widefield fluorescence Spinning Disk confocal channel modality,
514 imaging parameters included an excitation wavelength of 488 nm selected using the Full
515 Multiband Penta filter (DAPI/FITC/TRITC/Cy5/Cy7: 391/477/549/639/741), a laser intensity of
516 25%, and an exposure time of 150 ms. This configuration resulted in an emission wavelength of
517 684 nm collected using the Cy5 filter (685/40). Images were acquired using NIS Elements AR
518 5.42 software.
519
520 **Genomic extraction and whole genome sequencing analysis**
521 Genomic DNA from AB5075 was isolated using a EasyDNA genomic kit (Invitrogen) and subject
522 to Illumina Whole Genome Sequencing (SeqCenter, Pittsburgh). Mean genome coverage was
523 103.1-fold, (SD 17.8). Gene inactivations by transposon and background and potential suppressor
524 mutations were identified by use of the breseq pipeline (44), including Bowtie 2 for sequence
525 alignment (45), using the default settings. Because the source of the mutant library was the
526 ABUW_5075 transposon resource (40), genome file CP008706 of *A. baumannii* strain AB5075-
527 UW was used for sequence read alignment. Briefly, high-confidence mutations, flagged as
528 sequence reads differing from the reference alignment and missing coverage and new junctions
529 were assigned priority, if not present in the sequence of the parent strain, although marginal calls
530 or missing coverage were evaluated both visually and in the fastq files when present at high
531 frequency in the same gene or enzymatic pathway, when the same gene was mutated in more than
532 one independent clone, and specifically when the base change or changes would result in a drastic

533 change in the protein i.e., stop codons or change of reading frame were followed up, while
534 intergenic changes, synonymous codon changes and changes that would lead to similar amino acid
535 incorporation were not.
536
537 **Colony spot susceptibility assays**
538 Overnight cultures were serially diluted from 10^0 to 10^{-5} and spotted onto LB agar plates
539 containing varying concentrations of detergent (SDS or SDS/EDTA) or antibiotic (rifampin,
540 colistin or vancomycin). Plates were incubated at 37°C and growth was monitored to assess strain
541 susceptibility under each condition.
542
543 **Peptidoglycan isolation and muropeptide analysis**
544 AB5075 cultures were grown in 400 ml of LB medium until they reached either mid-logarithmic
545 or stationary phase. Cells were harvested at 4°C and resuspended in 6 ml of pre-chilled water. The
546 suspensions were dropped into 6 ml of boiling 8% SDS solution and boiled for 30 minutes.
547 Muropeptides were isolated using a previously established method (8). In short, peptidoglycan was
548 digested with the muramidase Cellosyl (Hoechst, Frankfurt am Main, Germany) to release
549 muropeptides, which were then reduced with sodium borohydride. Separation of the reduced
550 muropeptides was performed on a reversed-phase Prontosil 120-3-C18 AQ column (250 × 4.6 mm,
551 3 µm; Bischoff, Leonberg, Germany). The eluates were monitored at 205 nm by UV absorbance.
552 Peaks were identified by comparison with previously published chromatographic profiles of *A.*
553 *baumannii* 17978 (17,22,29), and novel peaks were further identified through tandem mass
554 spectrometry (MS/MS). For each condition, mean values and variability were determined from
555 two independent biological replicates.

556

557 **Generation of PBP1A-FLAG and LdtJ-FLAG fusion constructs**

558 The primers used to generate PBP1A-FLAG and LdtJ-FLAG are listed in Table S3. The *mrcA*
559 gene encoding PBP1A and the *ldtJ* gene encoding LdtJ from *A. baumannii* 17978 were amplified,
560 purified, and cloned into the KpnI/BamHI sites of $pMMB^{KanR}$ (17) to create pPBP1A-FLAG and
561 pLdtJ-FLAG, respectively. Plasmids were then transformed into wild type cells and the respective
562 single mutants, and the gene expression was induced with 1mM IPTG for co-immunoprecipitation.

563

564 **Co-immunoprecipitation and Western blotting**

565 As previously described (46), overnight cultures were diluted to an initial optical density of OD_{600}
566 0.05 in 400 ml of LB broth and grown to late-logarithmic phase (OD_{600} ~0.9) at 37°C. Cells from
567 100 ml culture were harvested, washed with 1X PBS, and incubated with 25 mM dithiobis-
568 succinimidyl propionate (DSP, Thermo Fisher Scientific) cross-linker in 1 ml PBS for 1 hour in
569 shaking conditions at 37°C. The reaction was quenched by incubation at room temperature with
570 400 µl of 1 M glycine with rocking for 15 minutes. Cells were then lysed and solubilized overnight
571 at 4°C with rocking. Lysates were centrifuged at 10000 x g for 20 minutes and the supernatant was
572 centrifuged twice to completely remove the pellet. 30 µl of anti-FLAG M2 affinity resin (Sigma)
573 was added to the supernatant and incubated overnight at 4°C with rocking. The resin was then
574 collected by centrifugation at 6000 x g for 15 minutes and washed 4 times with
575 radioimmunoprecipitation assay (RIPA) buffer. Bound proteins were eluted by resuspending the
576 resin in 100 µl SDS-PAGE loading buffer supplemented with 5% β-mercaptoethanol (BME),
577 followed by boiling at 95°C for 7 minutes and samples were used for Western blotting.

578 Western blotting was performed by transferring proteins onto polyvinylidene fluoride
579 (PVDF) membranes (Thermo Fisher Scientific). Membranes were blocked with 5% milk for
580 2 hours, followed by incubation with primary antibodies α-FLAG (1:1000), α- PBP1A (1:1000),
581 α- LdtJ (1:500), α- 6×His (1:500), and α- RpoA (1:1000). Detection was carried out using
582 horseradish peroxidase (HRP)-conjugated secondary antibodies: anti-rat HRP (1:10000; Thermo
583 Fisher Scientific) for anti-FLAG, and anti-rabbit HRP (1:10000; Thermo Fisher Scientific) for all
584 other primary antibodies.
585
586 **Isolation of LOS⁻ *A. baumannii* and determination of mutation frequency.** Isolation of LOS⁻
587 *A. baumannii* colonies was performed as described previously (17,22). Overnight cultures at OD_{600}
588 of 1.0 (~10^9 CFU) were harvested by centrifugation at 8,000 rpm for 2 min, washed once with 1
589 ml of LB broth, and plated on LB agar supplemented with colistin (10 µg/ml). After overnight
590 incubation, isolated colistin-resistant colonies were repatched onto LB agar containing
591 vancomycin (10 µg/ml), colistin (10 µg/ml), and no antibiotic as control. Colonies resistant to
592 colistin but sensitive to vancomycin were considered LOS-. The LOS- recovery frequency was
593 calculated as the ratio of LOS- colonies to the colony forming units count in 100 µl.
594
595 **LOS staining and analysis.** LOS analysis was done as previously reported (42). Overnight
596 cultures were diluted to an OD_{600} of 0.1 in 5 ml LB broth and grown at 37°C with shaking until
597 reaching an OD_{600} of ~1. 1 ml of cells were harvested and resuspended in 100 µl 1X Sample Buffer
598 (prepared from 4X LDS Sample Buffer, 4% β-mercaptoethanol, and water) and boiled for
599 10 minutes before incubating at 55°C overnight with proteinase K. The following day, samples

600 were boiled for 10 minutes and subjected to SDS-PAGE. Gels were fixed and stained following
601 the Pro-Q Emerald 300 Lipopolysaccharide Gel Stain Kit (Thermo Fisher Scientific, P20495).
602
603 **Determination of minimal inhibitory concentrations (MICs).** MIC determination was done as
604 previously described (47), using E-test strips (Liofilchem). The Δ*ldtJ* Δ*mrcA* colistin-resistant
605 LOS- overnight culture was concentrated 10X and spread uniformly on LB agar plates using a
606 sterile cotton swab, completely covering of the agar surface. Once the plates dried, an E-test strip
607 was placed onto the surface in sterile conditions. Plates were incubated at 37°C for 18–20 hours.
608

609 **Acknowledgments**

610 We thank Alessandra Polissi and Alessandra Martorana for stimulating ideas and discussion. We
611 would also like to thank Jason Peters and his laboratory for sharing the hygromycin replicative
612 plasmids for complementation in AB5075. We thank Philip Rather and his laboratory for
613 generously sharing their *Acinetobacter baumannii* AB5075 mutagenesis and natural
614 transformation protocols, which facilitated construction of the mutants used in this study.
615 Work in the O.M. lab was supported by the internal funding from the Interdisciplinary Center for
616 Medical Sciences (CISMed) to O.M. Work in the J.M.B. lab was supported by the National
617 Institutes of Health grants R01AI168159 and R35GM143053. Work in the W.V. lab was supported
618 by the NIH grant R01AI168159. The work of B.F. was also supported by the FEMS Research and
619 Training Grant.
620 B.F., S.N., H.G., M.B.W., W.V., J.M.B, and O.M. participated in the conception or design of the
621 study; B.F., S.N., H.G., M.B.W., N.M., R.J.O.O, D.V., W.V., J.M.B. and O.M. participated in the

622 acquisition, analysis, or interpretation of the data; B.F., S.N. and R.J.O.O. wrote the manuscript;
623 and W.V., J.M.B. and O.M. made comments on and revisions to the manuscript.
624
625
626 **Figure legends**
627 **Figure 1. Characterization of the *A. baumannii* AB5075 Δ*ldtJ* Δ*mrcA* double mutant.**
628 **(A)** Growth (OD_{600}) and (B) viability (CFU/ml) of wild type (WT), Δ*ldtJ*, Δ*mrcA*, and Δ*ldtJ*
629 Δ*mrcA* mutants in LB. Each experiment was independently performed in triplicate. (C) Phase-
630 contrast and D-amino acid (HADA) fluorescence microscopy of the WT and mutants in
631 logarithmic phase of growth. (D) Quantification of cell length, width, aspect ratio, and HADA
632 fluorescence intensity (n >100 cells per strain), analyzed using ImageJ software. Statistical
633 significance was determined using one-way ANOVA (**P < 0.01; ****P < 0.0001; ns = not
634 significant)
635
636 **Figure 2. Defects of the Δ*ldtJ* Δ*mrcA* double mutant in OM permeability and integrity.**
637 Colony spot susceptibility assays of *A. baumannii* AB5075 WT, Δ*ldtJ*, Δ*mrcA* single mutants, and
638 the Δ*ldtJ* Δ*mrcA* double mutant. Serial dilutions spotted on A) LB agar containing increasing
639 concentrations of Rifampin and B) LB agar containing 0.0625% SDS or 0.03% SDS/0.15 mM
640 EDTA.
641
642 **Figure 3. Peptidoglycan structure is altered in the Δ*ldtJ* Δ*mrcA* double mutant. (A)**
643 Chromatograms showing PG composition of *A. baumannii* AB5075 WT, Δ*ldtJ*, Δ*mrcA* and the
644 Δ*ldtJ* Δ*mrcA* mutants in logarithmic phase analyzed by HPLC. **(B)** Degree of 3-4 and 3-3 cross-

645 links and **(C)** Percentage of total anhydro shortened chains. Error bars indicate variation of two
646 biological replicates.
647
648 **Figure 4. PBP1A directly interacts with LdtJ.** Immunoblotting of the whole-cell lysates (WCL)
649 controls and co-immunoprecipitation (Co-IP) fractions from *A. baumannii* ATCC 17978 wild type
650 and Δ*mrcA* mutants expressing LdtJ-FLAG (1 and 2). LdtJ-FLAG was immunoprecipitated using
651 anti-FLAG resin. Immunoblotting with anti-PBP1A antibody detected PBP1A specifically in LdtJ-
652 FLAG pull-downs, indicating an interaction. Reciprocal Co-IP of PBP1A-FLAG expressed in WT
653 or Δ*ldtJ* similarly co-precipitated LdtJ, confirming the association (3 and 4). PBP1A and LdtJ were
654 detected with specific anti-PBP1A and anti-LdtJ antisera, LdtJ-FLAG and PBP1A-FLAG were
655 detected using anti-FLAG monoclonal antibodies. RpoA (RNA polymerase α-subunit), also
656 detected with a specific antiserum, was used as a cytoplasmic contamination control, confirming
657 the specificity of the Co-IP fractions. PBP1A is 94.7 kDa; LdtJ is 44.5 kDa; FLAG tag is 1 kDa;
658 RpoA is 37.6 kDa.
659
660 **Figure 5. Isolation and characterization of the ColR LOS⁻ variants in the Δ*ldtJ* Δ*mrcA* double**
661 **mutant. (A)** Recovery frequencies of Col-R colonies from *A. baumannii* 5075 WT, Δ*ldtJ*, Δ*mrcA,*
662 Δ*mrcB* single mutants and Δ*ldtJ* Δ*mrcA* and Δ*ldtJ* Δ*mrcB* double mutants. Recovery frequency of
663 Δ*ldtJ* Δ*mrcA* and Δ*ldtJ* Δ*mrcB* Col-R colonies are the average values of two independent isolates
664 for each mutant. *N/A: no Col-R LOS- isolates recovered. **(B)** LOS staining of the *A.*
665 *baumannii* 5075 WT, Δ*ldtJ*, Δ*mrcA* single and the Δ*ldtJ* Δ*mrcA* COL-S and COL-R double
666 mutants. **(C)** Colony spot assay of the Δ*ldtJ* Δ*mrcA* Col-S LOS+ parent and Col-R LOS⁻ derivative
667 on LB agar and LB agar supplemented with Colistin (10 µg/ml) or Vancomycin (10 µg/ml).

668 **(D)** Antibiotic susceptibility profile of the AB5075 Δ*ldtJ* Δ*mrcA* ColS LOS+ parent and ColR
669 LOS⁻ derivative for Colistin and selected OM low-permeability antibiotics. **(E)** Growth curves of
670 AB5075 WT, the Δ*ldtJ* Δ*mrcA* Col-S LOS+ parent and the Δ*ldtJ* Δ*mrcA*.
671
672
673 **Supplementary Figure and Tables legends**
674 **Figure S1. Whole-genome sequencing of *A. baumannii* AB5075 WT, Δ*ldtJ,* Δ*mrcA* and Δ*ldtJ***
675 **Δ*mrcA* double mutants.** Whole-genome sequencing was performed to confirm the simultaneous
676 inactivation of the *ldtJ* and *mrcA* genes and to verify the absence of suppressor mutations in the
677 Δ*ldtJ* Δ*mrcA* double mutants. **(A)** Read coverage depth across the *ldtJ* locus. **(B)** Read coverage
678 depth across the *mrcA* locus. Both Δ*ldtJ* Δ*mrcA* #1 and *ldtJ* Δ*mrcA* #2 mutants showed an insertion
679 (*tn* or *tnlox*) in the *ldtJ* locus and *mrcA* locus, confirming double inactivaction of *ldtJ* and *mrcA*.
680
681 **Figure S2. Characterization of the *A. baumannii* AB5075 Δ*ldtJ* Δ*mrcB* double mutant. (A)**
682 Growth (OD_{600}) and **(B)** viability (CFU/ml) of wild type (WT), Δ*ldtJ*, Δ*mrcB,* and Δ*ldtJ* Δ*mrcB*
683 mutants in LB. Each experiment was independently performed in triplicate. **(C)** Phase-contrast
684 and D-amino acid (HADA) fluorescence microscopy of the WT and mutants in logarithmic phase
685 of growth. **(D)** Quantification of cell length, width, aspect ratio, and HADA fluorescence intensity
686 of each population (n >100 cells per strain), analyzed using ImageJ software. Statistical
687 significance was determined using one-way ANOVA (*$P < 0.05$; ***$P < 0.001$; ****$P < 0.0001$;
688 ns = not significant).
689

690 **Figure S3. Characterization of the *A. baumannii* ATCC 17978 Δ*ldtJ* Δ*mrcA* double mutant.**
691 **(A)** Growth (OD_{600}) of wild type (WT), Δ*ldtJ*, Δ*mrcA,* and Δ*ldtJ* Δ*mrcA* mutants in LB. Each
692 experiment was independently performed in triplicate. **(B)** Phase-contrast and D-amino acid
693 (HADA) fluorescence microscopy of the WT, Δ*ldtJ*, Δ*mrcA*, and Δ*ldtJ* Δ*mrcA* mutants. **(C)**
694 Quantification of cell length, width, aspect ratio, and HADA fluorescence intensity of each
695 population (n >100 cells per strain), analyzed using ImageJ software. Statistical significance was
696 determined using one-way ANOVA (*$P < 0.05$; **$P < 0.01$; ***$P < 0.001$; ****$P < 0.0001$; ns =
697 not significant).
698
699 **Figure S4. Ectopic production of PBP1A or LdtJ in the *A. baumannii* AB5075 and ATCC**
700 **17978 Δ*ldtJ* Δ*mrcA* double mutants restore the respective single mutants phenotype. (A)**
701 Phase-contrast and HADA fluorescence microscopy of the AB5075 Δ*ldtJ* Δ*mrcA* double mutant
702 transformed either with the empty vector (pEV) or the plasmids expressing *mrcA* (pPBP1A) or
703 *ldtJ* (pLdtJ) in logarithmic phase of growth. **(B)** Phase-contrast and HADA fluorescence
704 microscopy of the ATCC 17978 Δ*ldtJ* Δ*mrcA* double mutant transformed either with the empty
705 vector (pEV) or the plasmids expressing *mrcA* (pPBP1A) or *ldtJ* (pLdtJ) in logarithmic phase of
706 growth.
707
708 **Figure S5. Ectopic production of PBP1a or LdtJ in the *A. baumannii* AB5075 Δ*ldtJ* Δ*mrcA***
709 **double mutant restore the ability to grow in the presence of rifampin.** Colony spot assay of
710 the Δ*ldtJ* Δ*mrcA* double mutant carrying pEV, pLdtJ or pPBP1A on LB agar with or without 0.562
711 μg/ml rifampin.
712

713 **Figure S6. Cross-linkage changes are maintained in stationary phase. (A)** PG isolated from *A.*
714 *baumannii* AB5075 Δ*ldtJ*, Δ*mrcA* and the Δ*ldtJ* Δ*mrcA* mutants in stationary phases was analyzed
715 by High Performance Liquid Chromatography (HPLC). **(B)** Schematic representation of 4-3 and
716 3-3 cross-links.
717
718 **Table S1:** Muropeptide composition of wild type, Δ*ldtJ*, Δ*mrcA* and Δ*ldtJ* Δ*mrcA* in *A. baumannii*
719 strain AB5075.
720
721 **Table S2:** Strains and plasmids used in this study.
722
723 **Table S3:** Primers used in this study.
724
725 **References**

726 1. Woodford N, Turton JF, Livermore DM. Multiresistant Gram-negative bacteria: The role of
727 high-risk clones in the dissemination of antibiotic resistance. FEMS Microbiol Rev. 2011;
728 35(5):736–55.

729 2. Li J, Rayner CR, Nation RL, Owen RJ, Spelman D, Tan KE, et al. Heteroresistance to colistin
730 in multidrug-resistant *Acinetobacter baumannii*. Antimicrob Agents Chemother. 2006;
731 50(9):2946–50.

732 3. Silhavy TJ, Kahne D, Walker S. The bacterial cell envelope. Cold Spring Harb Perspect Biol.
733 2010; 2(5):a000414.

734 4. Boll JM, Tucker AT, Klein DR, Beltran AM, Brodbelt JS, Davies BW, et al. Reinforcing lipid
735 A acylation on the cell surface of *Acinetobacter baumannii* promotes cationic antimicrobial
736 peptide resistance and desiccation survival. mBio. 2015; 6(3):e00478-15.

737 5. Moffatt JH, Harper M, Harrison P, Hale JDF, Vinogradov E, Seemann T, et al. Colistin
738 resistance in *Acinetobacter baumannii* is mediated by complete loss of lipopolysaccharide
739 production. Antimicrob Agents Chemother. 2010; 54(12):4971–7.

740 6. Egan AJF, Errington J, Vollmer W. Regulation of peptidoglycan synthesis and remodelling. Nat
741 Rev Microbiol. 2020; 18(8):446–60.

742 7. Vollmer W, Blanot D, De Pedro MA. Peptidoglycan structure and architecture. FEMS
743 Microbiol Rev. 2008; 32(2):149–67.

744 8. Glauner B, Höltje JV, Schwarz U. The composition of the murein of *Escherichia coli*. J Biol
745 Chem. 1988; 263(21):10088–95.

746 9. Aliashkevich A, Cava F. LD-transpeptidases: the great unknown among the peptidoglycan
747 cross-linkers. FEBS J. 2022; 289(16):4718–30.

748 10. Mainardi JL, Legrand R, Arthur M, Schoot B, Van Heijenoort J, Gutmann L. Novel
749 mechanism of β-Lactam resistance due to bypass of DD-transpeptidation in *Enterococcus*
750 *faecium*. J Biol Chem. 2000; 275(22):16490–6.

751 11. Mainardi JL, Morel V, Fourgeaud M, Cremniter J, Blanot D, Legrand R, et al. Balance between
752 two transpeptidation mechanisms determines the expression of β-lactam resistance in
753 *Enterococcus faecium*. J Biol Chem. 2002; 277(39):35801–7.

754 12. Mainardi JL, Fourgeaud M, Hugonnet JE, Dubost L, Brouard JP, Ouazzani J, et al. A novel
755 peptidoglycan cross-linking enzyme for a β-lactam-resistant transpeptidation pathway. J Biol
756 Chem. 2005; 280(46):38146–52.

757 13. Hugonnet JE, Mengin-Lecreulx D, Monton A, Den Blaauwen T, Carbonnelle E, Veckerlé C,
758 et al. Factors essential for L,D-transpeptidase-mediated peptidoglycan cross-linking and β-
759 lactam resistance in *Escherichia coli*. eLife. 2016; 5:e19469.

760 14. De Pedro MA, Cava F. Structural constraints and dynamics of bacterial cell wall architecture.
761 Front Microbiol. 2015; Volume 8:6:449.

762 15. Morè N, Martorana AM, Biboy J, Otten C, Winkle M, Serrano CKG, et al. Peptidoglycan
763 remodeling enables *Escherichia coli* to survive severe outer membrane assembly defect. mBio.
764 2019; 10(1):e02729-18.

765 16. Gastrell S, Vollmer W. Peptidoglycan LD-Transpeptidases. Antibiotics. 2025; 14(12):1210.

766 17. Kang KN, Kazi MI, Biboy J, Gray J, Bovermann H, Ausman J, et al. Septal class A penicillin-
767 binding protein activity and LD-transpeptidases mediate selection of colistin-resistant
768 lipooligosaccharide-deficient *Acinetobacter baumannii*. mBio. 2021; 12(1):e02185-20.

769 18. Dai Y, Pinedo V, Tang AY, Cava F, Geisinger E. A new class of cell wall-recycling L,D-
770 carboxypeptidase determines β-lactam susceptibility and morphogenesis in *Acinetobacter*
771 *baumannii.* mBio. 2021;12(6):e0278621.

772 19. Nandy S, Tehrani AF, Hunt-Serracin AC, Biboy J, Pybus C, Vollmer W, et al. Molecular
773 interplay between peptidoglycan integrity and outer membrane asymmetry in maintaining cell
774 envelope homeostasis. J Bacteriol. 2025; 207:e0033125.

775 20. Kang KN, Boll JM. PBP1A directly interacts with the divisome complex to promote septal
776 peptidoglycan synthesis in *Acinetobacter baumannii*. J Bacteriol. 2022; 204:e0023922.

21. Clausell A, Garcia-Subirats M, Pujol M, Busquets MA, Rabanal F, Cajal Y. Gram-negative outer and inner membrane models: insertion of cyclic cationic lipopeptides. J Phys Chem B. 2007; 111(3):551–63.

22. Boll JM, Crofts AA, Peters K, Cattoir V, Vollmer W, Davies BW, et al. A penicillin-binding protein inhibits selection of colistin-resistant, lipooligosaccharide-deficient *Acinetobacter baumannii*. Proc Natl Acad Sci U S A. 2016; 113(41):E6228–37.

23. Sabnis A, Hagart KL, Klöckner A, Becce M, Evans LE, Furniss RCD, et al. Colistin kills bacteria by targeting lipopolysaccharide in the cytoplasmic membrane. eLife. 2021; 10:e65836.

24. Peters DL, Davis CM, Harris G, Zhou H, Rather PN, Hrapovic S, Lam E, Dennis JJ, Chen W. Characterization of virulent T4-like *Acinetobacter baumannii* bacteriophages DLP1 and DLP2. Viruses. 2023, 15(3):739.

25. Fivenson EM, Rohs PDA, Vettiger A, Sardis MF, Torres G, Forchoh A, et al. A role for the Gram-negative outer membrane in bacterial shape determination. Proc Natl Acad Sci USA. 2023; 120(35):e2301987120.

26. Han ML, Alsaadi Y, Zhao J, Zhu Y, Lu J, Jiang X, et al. Arginine catabolism is essential to polymyxin dependence in *Acinetobacter baumannii*. Cell Rep. 2024; 43(7):114410.

27. Zhu Y, Lu J, Han M, Jiang X, Azad MAK, Patil NA, et al. Polymyxins bind to the cell surface of unculturable *Acinetobacter baumannii* and cause unique dependent resistance. Adv Sci. 2020; 7(15):2000704.

28. Geisinger E, Mortman NJ, Dai Y, Cokol M, Syal S, Farinha A, et al. Antibiotic susceptibility signatures identify potential antimicrobial targets in the *Acinetobacter baumannii* cell envelope. Nat Commun. 2020; 11:4522.

29. Islam N, Kazi MI, Kang KN, Biboy J, Gray J, Ahmed F, et al. Peptidoglycan recycling promotes outer membrane integrity and carbapenem tolerance in *Acinetobacter baumannii*. mBio. 2022; 13:e0100122.

30. Geisinger E, Mortman NJ, Vargas-Cuebas G, Tai AK, Isberg RR. A global regulatory system links virulence and antibiotic resistance to envelope homeostasis in *Acinetobacter baumannii*. PLoS Pathog. 2018; 14:e1007030.

31. Juan C, Torrens G, Barceló IM, Oliver A. Interplay between peptidoglycan biology and virulence in Gram-negative pathogens. Microbiol Mol Biol Rev. 2018; 82:e00033-18.

32. Pisabarro AG, De Pedro MA, Vázquez D. Structural modifications in the peptidoglycan of *Escherichia coli* associated with changes in the state of growth of the culture. J Bacteriol. 1985; 161(1):238–42.

33. Typas A, Banzhaf M, Gross CA, Vollmer W. From the regulation of peptidoglycan synthesis to bacterial growth and morphology. Nat Rev Microbiol. 2012; 10(2):123–36.

813 34. Vollmer W, Bertsche U. Murein (peptidoglycan) structure, architecture and biosynthesis in
814 *Escherichia coli*. Biochim Biophys Acta BBA - Biomembr. 2008; 1778(9):1714–34.

815 35. Cava F, De Pedro MA, Lam H, Davis BM, Waldor MK. Distinct pathways for modification
816 of the bacterial cell wall by non-canonical D-amino acids: Distinct pathways for cell wall
817 remodelling. EMBO J. 2011; 30(16):3442–53.

818 36. Magnet S, Bellais S, Dubost L, Fourgeaud M, Mainardi JL, Petit-Frère S, et al. Identification
819 of the L,D-transpeptidases responsible for attachment of the Braun lipoprotein to *Escherichia*
820 *coli* peptidoglycan. J Bacteriol. 2007; 189(10):3927–31.

821 37. Deghelt M, Cho SH, Sun J, Govers SK, Janssens A, Dachsbeck AV, et al. Peptidoglycan–outer
822 membrane attachment generates periplasmic pressure to prevent lysis in Gram-negative
823 bacteria. Nat Microbiol. 2025; 10(8):1963–74.

824 38. Caveney NA, Caballero G, Voedts H, Niciforovic A, Worrall LJ, Vuckovic M, et al. Structural
825 insight into YcbB-mediated beta-lactam resistance in *Escherichia coli*. Nat Commun. 2019;
826 10(1):1849.

827 39. Nagy E, Losick R, Kahne D. Robust suppression of lipopolysaccharide deficiency in
828 *Acinetobacter baumannii* by growth in minimal medium. J Bacteriol. 2019; 201(22):e00420-
829 19.

830 40. Gallagher LA, Ramage E, Weiss EJ, Radey M, Hayden HS, Held KG, et al. Resources for
831 genetic and genomic analysis of emerging pathogen *Acinetobacter baumannii*. J Bacteriol.
832 2015; 197(12):2027–35.

833 41. Bacon EE, Tran JS, Nadig N, Peters JM. Modular, inducible, and titratable expression systems
834 for *Escherichia coli* and *Acinetobacter baumannii*. Microbiol Spectr. 2024; 12(11):e01306-
835 24.

836 42. Olea-Ozuna RJ, Campbell MJ, Quintanilla SY, Nandy S, Brodbelt JS, Boll JM. Alternative
837 lipid synthesis in response to phosphate limitation promotes antibiotic tolerance in Gram-
838 negative ESKAPE pathogens. PLoS Pathog. 2025; 21(2):e1012933.

839 43. Podolsky T, Fong ST, Lee BTO. Direct selection of tetracycline-sensitive *Escherichia coli*
840 cells using nickel salts. Plasmid. 1996; 36(2):112–5.

841 44. Deatherage DE, Barrick JE. Identification of mutations in laboratory-evolved microbes from
842 next-generation sequencing data using *breseq*. In Engineering and analyzing multicellular
843 systems: methods and protocols 2014 Apr 17 (pp. 165-188). New York, NY: Springer New
844 York.

845 45. Langmead B, Salzberg SL. Fast gapped-read alignment with Bowtie 2. Nat Methods. 2012;
846 9(4):357–9.

847 46. Boll JM, Hendrixson DR. A regulatory checkpoint during flagellar biogenesis in
848 *Campylobacter jejuni* initiates signal transduction to activate transcription of flagellar genes.
849 mBio. 2013; 4(5):e00432-13.

850 47. Powers MJ, Trent MS. Phospholipid retention in the absence of asymmetry strengthens the
851 outer membrane permeability barrier to last-resort antibiotics. Proc Natl Acad Sci USA. 2018;
852 115(36):E8518-27.

853 **Figures**

854

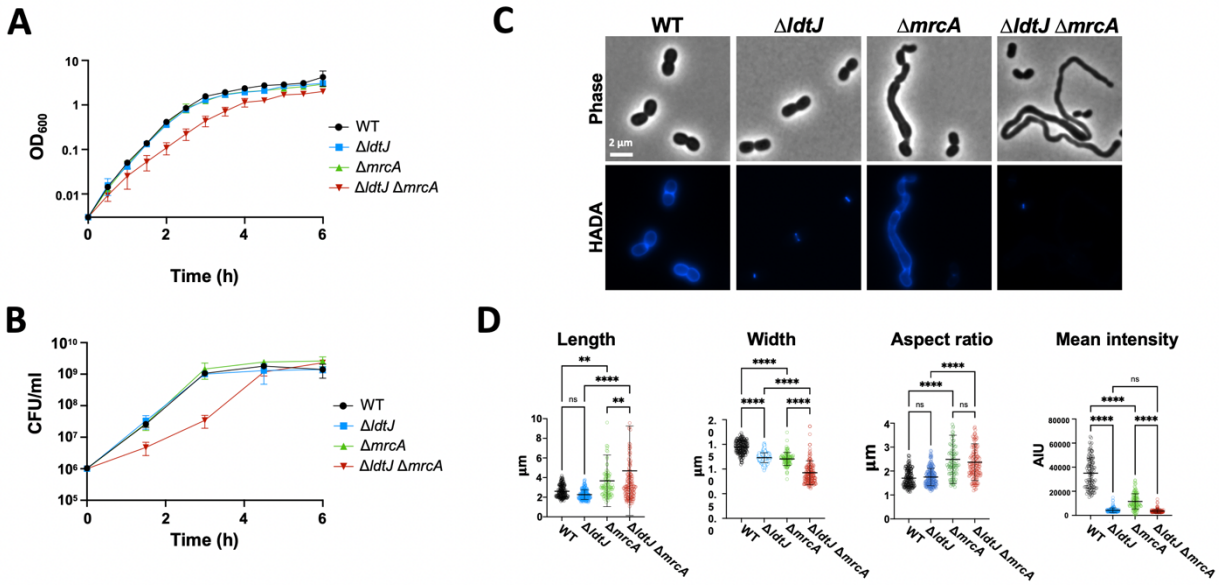

855

856

857 **Figure 1. Characterization of the *A. baumannii* AB5075 Δ*ldtJ* Δ*mrcA* double mutant.**

858 **(A)** Growth (OD_{600}) and (B) viability (CFU/ml) of wild type (WT), Δ*ldtJ*, Δ*mrcA*, and Δ*ldtJ*

859 Δ*mrcA* mutants in LB. Each experiment was independently performed in triplicate. (C) Phase-

860 contrast and D-amino acid (HADA) fluorescence microscopy of the WT and mutants in

861 logarithmic phase of growth. (D) Quantification of cell length, width, aspect ratio, and HADA

862 fluorescence intensity (n >100 cells per strain), analyzed using ImageJ software. Statistical

863 significance was determined using one-way ANOVA (**$P < 0.01$; ****$P < 0.0001$; ns = not

864 significant).

865

866

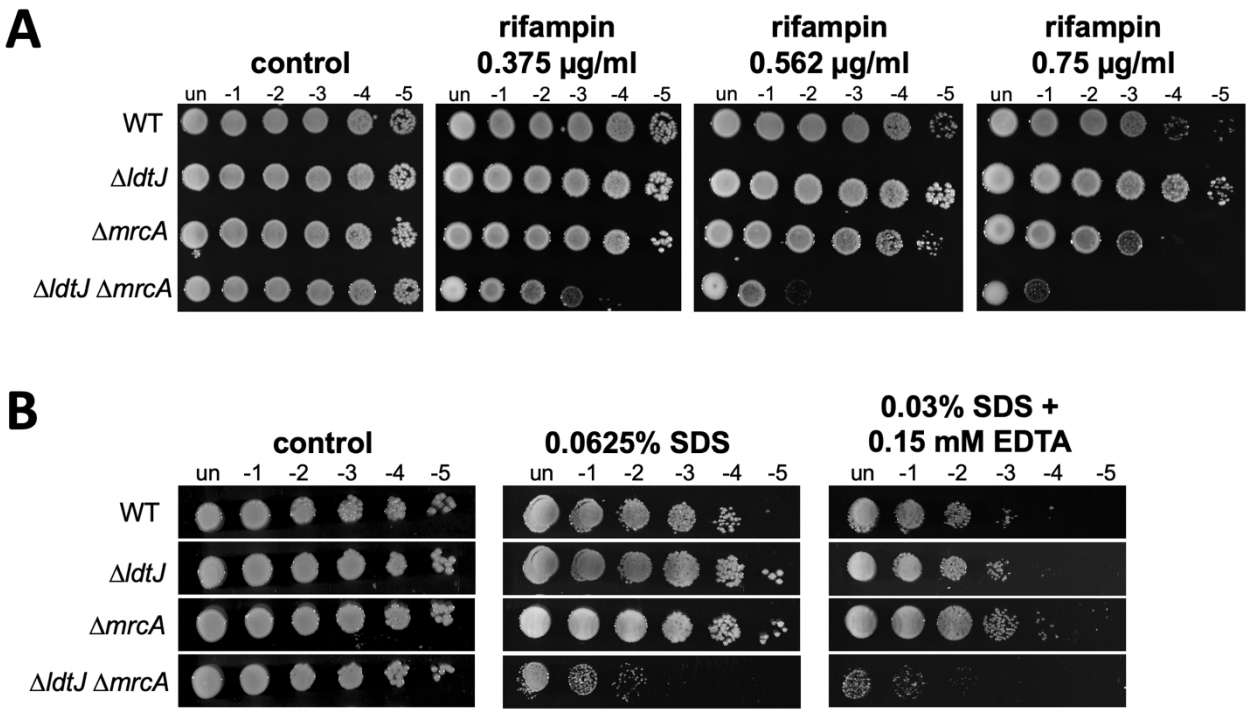

Figure 2. Defects of the Δ*ldtJ* Δ*mrcA* double mutant in OM permeability and integrity. Colony spot susceptibility assays of *A. baumannii* AB5075 WT, Δ*ldtJ*, Δ*mrcA* single mutants, and the Δ*ldtJ* Δ*mrcA* double mutant. Serial dilutions spotted on A) LB agar containing increasing concentrations of Rifampin and B) LB agar containing 0.0625% SDS or 0.03% SDS/0.15 mM EDTA.

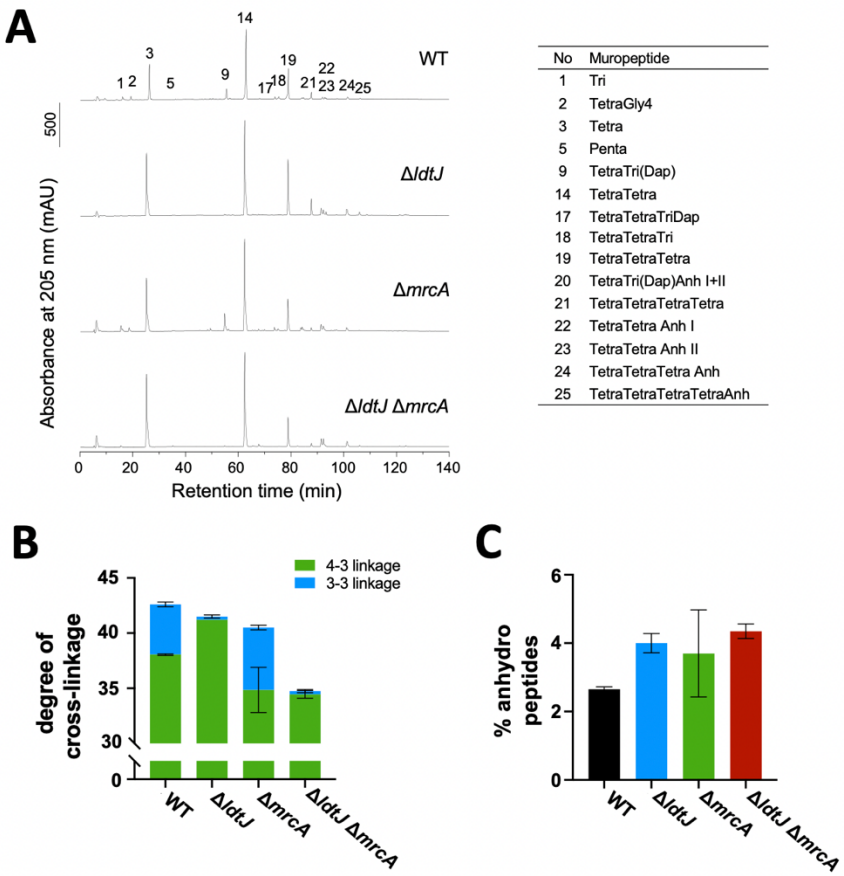

Figure 3. Peptidoglycan structure is altered in the Δ*ldtJ* Δ*mrcA* double mutant. (A) Chromatograms showing PG composition of *A. baumannii* AB5075 WT, Δ*ldtJ*, Δ*mrcA* and the Δ*ldtJ* Δ*mrcA* mutants in logarithmic phase analyzed by HPLC. **(B)** Degree of 3-4 and 3-3 cross-links and **(C)** Percentage of total anhydro shortened chains. Error bars indicate variation of two biological replicates.

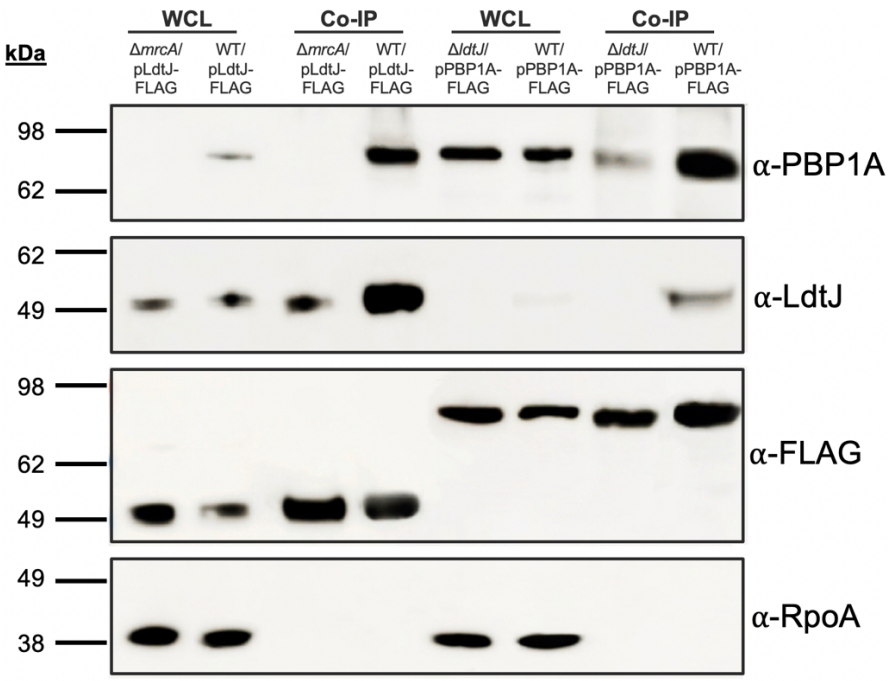

Figure 4. PBP1A directly interacts with LdtJ. Immunoblotting of the whole-cell lysates (WCL) controls and co-immunoprecipitation (Co-IP) fractions from *A. baumannii* ATCC 17978 wild type and Δ*mrcA* mutants expressing LdtJ-FLAG (1 and 2). LdtJ-FLAG was immunoprecipitated using anti-FLAG resin. Immunoblotting with anti-PBP1A antibody detected PBP1A specifically in LdtJ-FLAG pull-downs, indicating an interaction. Reciprocal Co-IP of PBP1A-FLAG expressed in WT or Δ*ldtJ* similarly co-precipitated LdtJ, confirming the association (3 and 4). PBP1A and LdtJ were detected with specific anti-PBP1A and anti-LdtJ antisera, LdtJ-FLAG and PBP1A-FLAG were detected using anti-FLAG monoclonal antibodies. RpoA (RNA polymerase α-subunit), also detected with a specific antiserum, was used as a cytoplasmic contamination control, confirming the specificity of the Co-IP fractions. PBP1A is 94.7 kDa; LdtJ is 44.5 kDa; FLAG tag is 1 kDa; RpoA is 37.6 kDa.

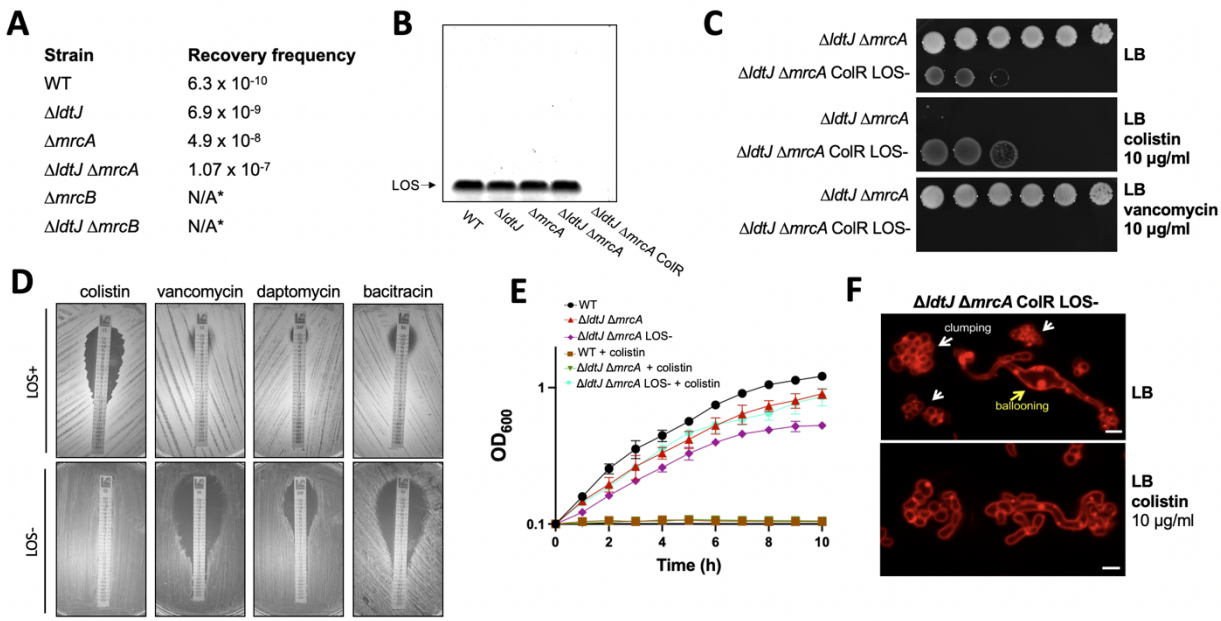

Figure 5. Isolation and characterization of the ColR LOS⁻ variants in the Δ*ldtJ* Δ*mrcA* double mutant. (A) Recovery frequencies of Col-R colonies from *A. baumannii* 5075 WT, Δ*ldtJ*, Δ*mrcA,* Δ*mrcB* single mutants and Δ*ldtJ* Δ*mrcA* and Δ*ldtJ* Δ*mrcB* double mutants. Recovery frequency of Δ*ldtJ* Δ*mrcA* and Δ*ldtJ* Δ*mrcB* Col-R colonies are the average values of two independent isolates for each mutant. *N/A: no Col-R LOS- isolates recovered. **(B)** LOS staining of the *A. baumannii* 5075 WT, Δ*ldtJ*, Δ*mrcA* single and the Δ*ldtJ* Δ*mrcA* COL-S and COL-R double mutants. **(C)** Colony spot assay of the Δ*ldtJ* Δ*mrcA* Col-S LOS+ parent and Col-R LOS⁻ derivative on LB agar and LB agar supplemented with Colistin (10 µg/ml) or Vancomycin (10 µg/ml). **(D)** Antibiotic susceptibility profile of the AB5075 Δ*ldtJ* Δ*mrcA* ColS LOS+ parent and ColR LOS⁻ derivative for Colistin and selected OM low-permeability antibiotics. **(E)** Growth curves of AB5075 WT, the Δ*ldtJ* Δ*mrcA* Col-S LOS+ parent and the Δ*ldtJ* Δ*mrcA*.

911 **Supplementary Figures**

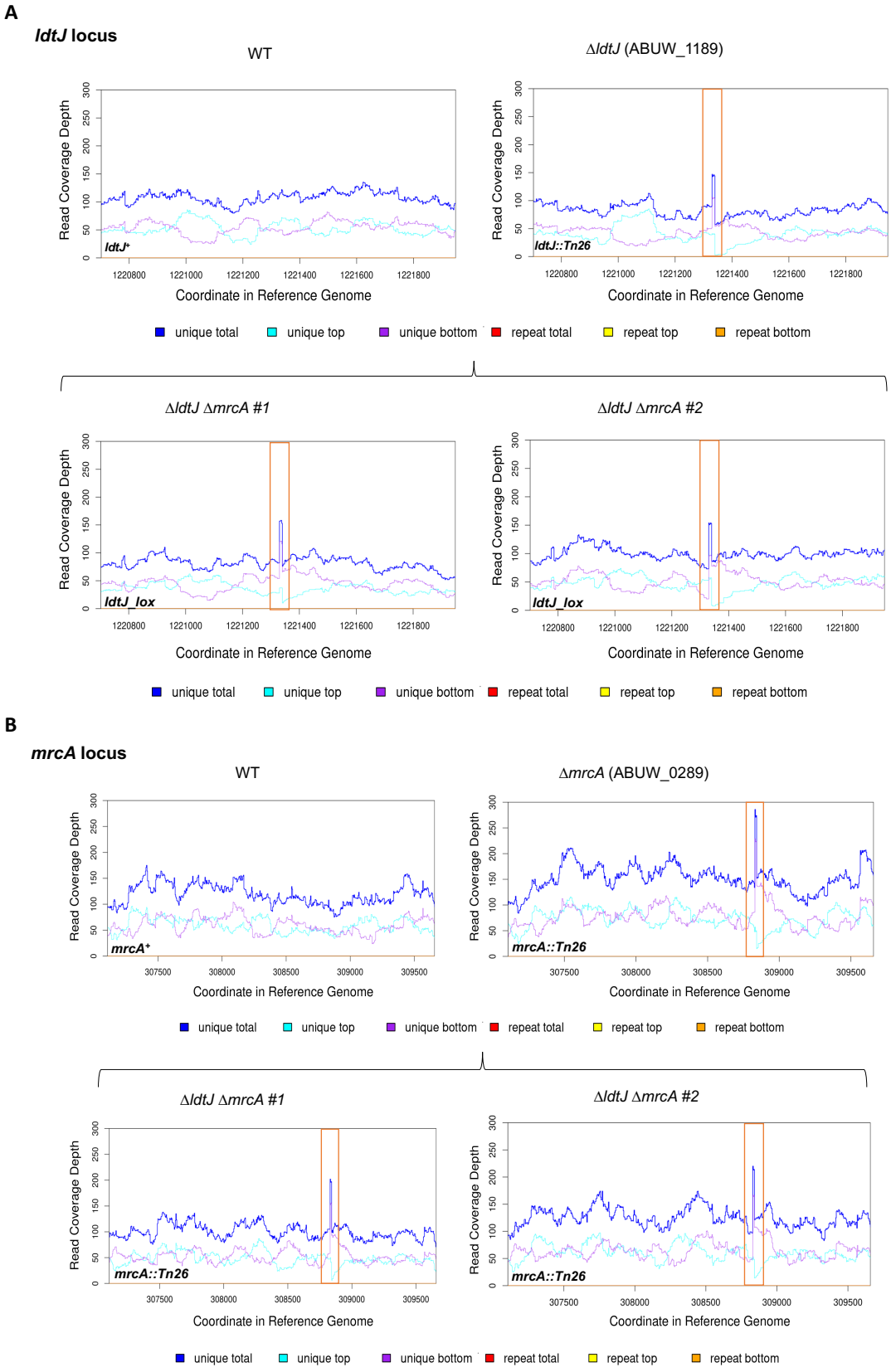

912

913 **Figure S1. Whole-genome sequencing of *A. baumannii* AB5075 WT, Δ*ldtJ*, Δ*mrcA* and Δ*ldtJ***

914 **Δ*mrcA* double mutants.** Whole-genome sequencing was performed to confirm the simultaneous

915 inactivation of the *ldtJ* and *mrcA* genes and to verify the absence of suppressor mutations in the

916 Δ*ldtJ* Δ*mrcA* double mutants. **(A)** Read coverage depth across the *ldtJ* locus. **(B)** Read coverage

917 depth across the *mrcA* locus. Both Δ*ldtJ* Δ*mrcA* #1 and *ldtJ* Δ*mrcA* #2 mutants showed an insertion

918 (*tn* or *tnlox*) in the *ldtJ* locus and *mrcA* locus, confirming double inactivation of *ldtJ* and *mrcA*.

919

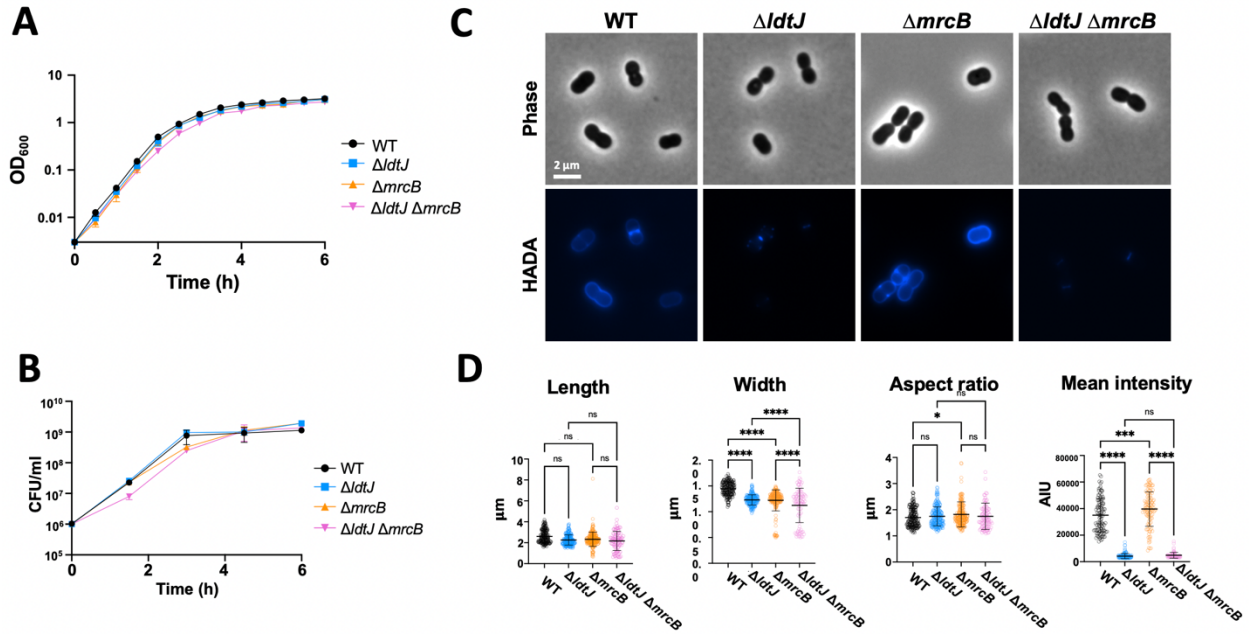

920

921

922 **Figure S2. Characterization of the *A. baumannii* AB5075 Δ*ldtJ* Δ*mrcB* double mutant. (A)**

923 Growth (OD_{600}) and **(B)** viability (CFU/ml) of wild type (WT), Δ*ldtJ*, Δ*mrcB,* and Δ*ldtJ* Δ*mrcB*

924 mutants in LB. Each experiment was independently performed in triplicate. **(C)** Phase-contrast

925 and D-amino acid (HADA) fluorescence microscopy of the WT and mutants in logarithmic phase

926 of growth. **(D)** Quantification of cell length, width, aspect ratio, and HADA fluorescence intensity

927 of each population (*n* >100 cells per strain), analyzed using ImageJ software. Statistical

928 significance was determined using one-way ANOVA (*$P < 0.05$; ***$P < 0.001$; ****$P < 0.0001$;

929 ns = not significant).

930

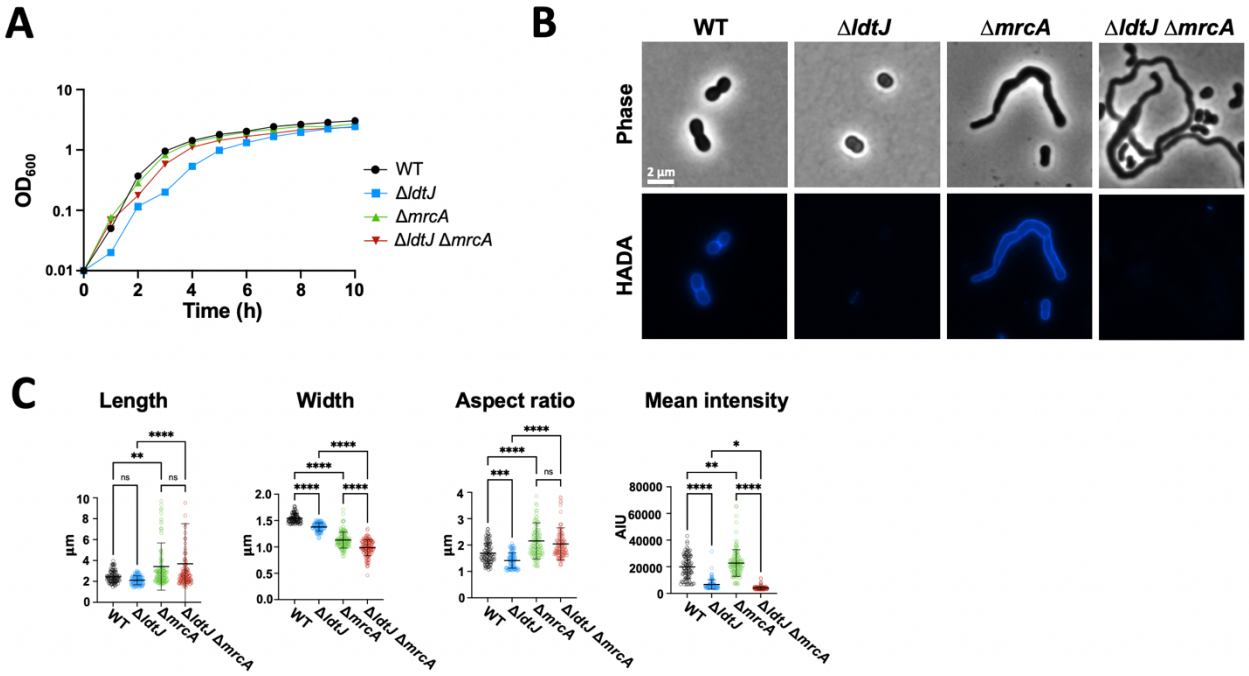

931

932

933 **Figure S3. Characterization of the *A. baumannii* ATCC 17978 Δ*ldtJ* Δ*mrcA* double mutant.**

934 **(A)** Growth (OD_{600}) of wild type (WT), Δ*ldtJ*, Δ*mrcA,* and Δ*ldtJ* Δ*mrcA* mutants in LB. Each

935 experiment was independently performed in triplicate. **(B)** Phase-contrast and D-amino acid

936 (HADA) fluorescence microscopy of the WT, Δ*ldtJ*, Δ*mrcA*, and Δ*ldtJ* Δ*mrcA* mutants. **(C)**

937 Quantification of cell length, width, aspect ratio, and HADA fluorescence intensity of each

938 population (n >100 cells per strain), analyzed using ImageJ software. Statistical significance was

939 determined using one-way ANOVA (*$P < 0.05$; **$P < 0.01$; ***$P < 0.001$; ****$P < 0.0001$; ns =

940 not significant).

941

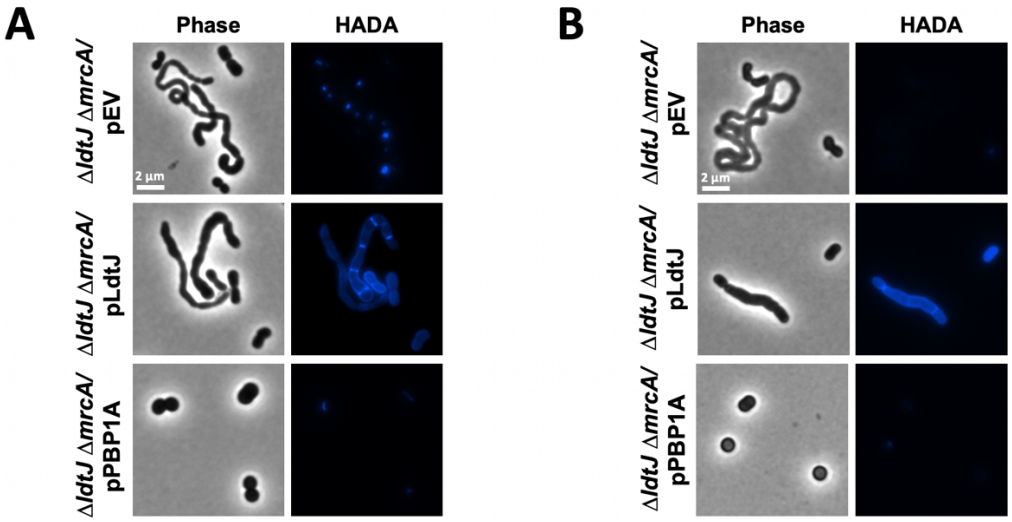

Figure S4. Ectopic production of PBP1A or LdtJ in the *A. baumannii* AB5075 and ATCC 17978 Δ*ldtJ* Δ*mrcA* double mutants restore the respective single mutants phenotype. (A) Phase-contrast and HADA fluorescence microscopy of the AB5075 Δ*ldtJ* Δ*mrcA* double mutant transformed either with the empty vector (pEV) or the plasmids expressing *mrcA* (pPBP1A) or *ldtJ* (pLdtJ) in logarithmic phase of growth. **(B)** Phase-contrast and HADA fluorescence microscopy of the ATCC 17978 Δ*ldtJ* Δ*mrcA* double mutant transformed either with the empty vector (pEV) or the plasmids expressing *mrcA* (pPBP1A) or *ldtJ* (pLdtJ) in logarithmic phase of growth.

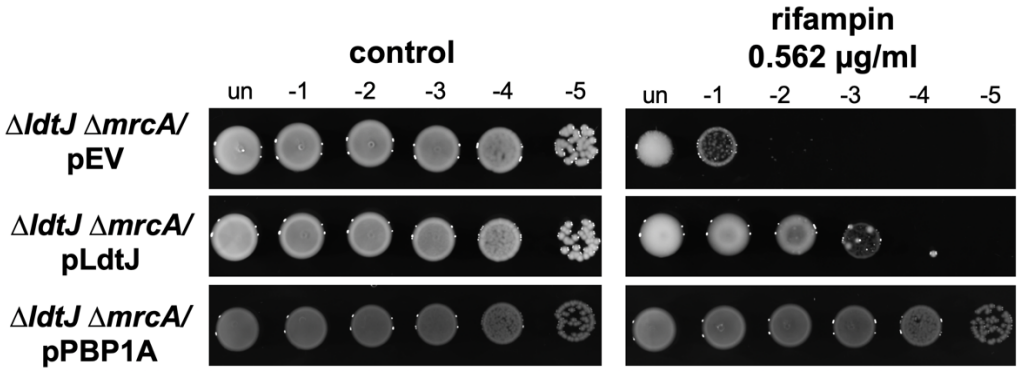

955 **Figure S5. Ectopic production of PBP1a or LdtJ in the *A. baumannii* AB5075 Δ*ldtJ* Δ*mrcA***

956 **double mutant restore the ability to grow in the presence of rifampin.** Colony spot assay of

957 the Δ*ldtJ* Δ*mrcA* double mutant carrying pEV, pLdtJ or pPBP1A on LB agar with or without 0.562

958 µg/ml rifampin.

959

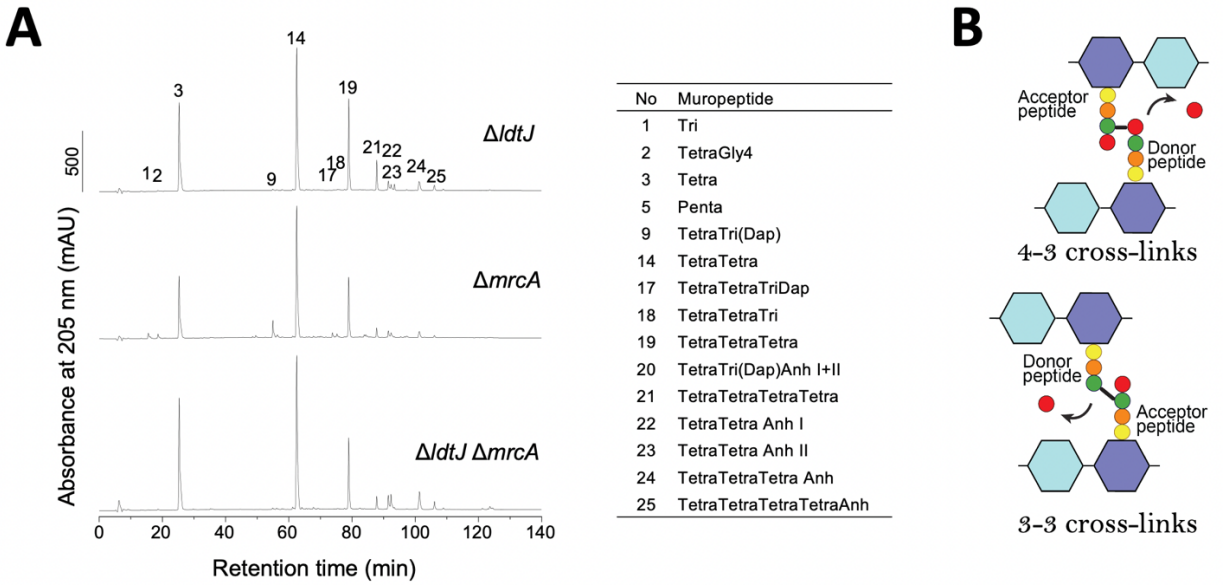

960

961

962 **Figure S6. Cross-linkage changes are maintained in stationary phase. (A)** PG isolated from *A.*

963 *baumannii* AB5075 Δ*ldtJ*, Δ*mrcA* and the Δ*ldtJ* Δ*mrcA* mutants in stationary phases was analyzed

964 by High Performance Liquid Chromatography (HPLC). **(B)** Schematic representation of 4-3 and

965 3-3 cross-links.

966

967 **Supplementary Tables**

968 **Table S1:** Muropeptide composition of wild type, Δ*ldtJ*, Δ*mrcA* and Δ*ldtJ* Δ*mrcA* in *A. baumannii*

969 strain AB5075.

Peak No.	Muropeptide	Relative % of each muropeptide[a]						
		WT Log	Δ*ldtJ* Log	Δ*ldtJ* Stat	Δ*mrcA* Log	Δ*mrcA* Stat	Δ*ldtJ* Δ*mrcA* Log	Δ*ldtJ* Δ*mrcA* Stat
1	Tri	2.0 ± 0.0	0.1 ± 0.0	0.0 ± 0.0	2.1 ± 0.2	1.4 ± 0.0	0.7 ± 0.0	0.0 ± 0.0
2	TetraGly 4	1.9 ± 0.0	0.1 ± 0.0	0.0 ± 0.0	1.2 ± 0.1	1.2 ± 0.0	0.0 ± 0.0	0.3 ± 0.0
3	Tetra	17.1 ± 0.2	25.1 ± 0.0	22.5 ± 0.1	19.0 ± 2.9	18.6 ± 1.4	32.5 ± 0.0	28.5 ± 0.0
4	Di	0.0 ± 0.0	0.0 ± 0.0	0.0 ± 0.0	0.0 ± 0.0	0.0 ± 0.0	0.0 ± 0.0	0.3 ± 0.0
5	Penta	0.1 ± 0.0	0.1 ± 0.0	0.0 ± 0.0	0.2 ± 0.0	0.2 ± 0.0	0.4 ± 0.0	0.3 ± 0.0
8	TriTri(DAP)	0.3 ± 0.0	0.0 ± 0.0	0.0 ± 0.0	0.7 ± 0.0	0.5 ± 0.0	0.0 ± 0.0	0.0 ± 0.0
9	TetraTri(DAP)	5.4 ± 0.0	0.5 ± 0.0	0.4 ± 0.0	6.8 ± 0.7	4.4 ± 0.0	0.3 ± 0.0	0.7 ± 0.0
14	TetraTetra	34.8 ± 0.1	37.6 ± 0.0	35.9 ± 1.1	38.5 ± 3.8	37.2 ± 0.0	40.6 ± 0.0	34.7 ± 0.0
15	TetraAnh	0.0 ± 0.0	0.3 ± 0.0	0.3 ± 0.0	0.0 ± 0.0	0.0 ± 0.0	0.0 ± 0.0	0.5 ± 0.0
16	TetraPenta	0.3 ± 0.0	0.3 ± 0.0	0.2 ± 0.0	0.6 ± 0.0	0.0 ± 0.0	0.8 ± 0.0	0.6 ± 0.0
17	TetraTetraTri(DAP)	1.2 ± 0.0	0.0 ± 0.0	0.0 ± 0.0	1.0 ± 0.0	1.0 ± 0.0	0.0 ± 0.0	0.0 ± 0.0
18	TetraTetraTri	1.6 ± 0.0	0.0 ± 0.0	0.0 ± 0.0	1.2 ± 0.2	1.0 ± 0.0	0.0 ± 0.0	0.0 ± 0.0
19	TetraTetraTetra	15.0 ± 0.0	17.2 ± 0.0	18.4 ± 0.0	10.9 ± 0.9	12.6 ± 0.5	9.5 ± 0.0	10.6 ± 0.0
20	TetraTri(DAP)Anh I	0.8 ± 0.0	0.0 ± 0.0	0.0 ± 0.0	0.8 ± 0.0	0.5 ± 0.0	0.0 ± 0.0	0.0 ± 0.0
20	TetraTri(DAP)Anh II	0.7 ± 0.0	0.0 ± 0.0	0.0 ± 0.0	1.4 ± 0.1	0.6 ± 0.0	0.0 ± 0.0	0.0 ± 0.0
21	TetraTetraTetraTetra	2.9 ± 0.0	4.4 ± 0.0	5.4 ± 0.1	1.1 ± 0.0	1.7 ± 0.0	0.9 ± 0.0	1.5 ± 0.0
22	TetraTetraAnh I	1.0 ± 0.0	2.3 ± 0.0	2.2 ± 0.0	1.9 ± 0.2	1.8 ± 0.0	2.9 ± 0.0	2.5 ± 0.0
23	TeraTetraAnh II	0.9 ± 0.0	1.7 ± 0.1	1.4 ± 0.0	1.7 ± 0.4	1.7 ± 0.0	3.5 ± 0.0	4.2 ± 0.0
24	TetraTetraTetra Anh	1.4 ± 0.0	3.3 ± 0.0	3.2 ± 0.0	1.5 ± 0.0	2.2 ± 0.0	2.9 ± 0.0	5.0 ± 0.0
25	TetraTetraTetraTetra Anh	0.5 ± 0.0	1.3 ± 0.0	1.3 ± 0.0	0.0 ± 0.0	0.5 ± 0.0	0.5 ± 0.0	1.4 ± 0.0
% known peaks		88.1±0.2	94.3 ± 0.0	91.3 ± 0.1	90.5 ± 0.1	87.3 ± 0.2	95.4 ± 0.0	91.1 ± 0.0
Monomers (Total)		24.0 ± 0.1	27.3 ± 0.0	25.0 ± 0.0	24.9 ± 7.1	24.5 ± 0.9	35.2 ± 0.0	32.8 ± 0.0
Monomers di		0.0 ± 0.0	0.0 ± 0.0	0.0 ± 0.0	0.0 ± 0.0	0.0 ± 0.0	0.0 ± 0.0	0.3 ± 0.0
Monomer tri		2.3 ± 0.0	0.1 ± 0.0	0.0 ± 0.0	2.3 ± 0.3	1.6 ± 0.1	0.7 ± 0.0	0.0 ± 0.0
Monomer tetra		19.4 ± 0.1	27.0 ± 0.0	25.0 ± 0.0	21.0 ± 3.8	21.3 ± 1.5	34.1 ± 0.0	31.8 ± 0.0
Monomer tetra-Gly4		2.1 ± 0.0	0.1 ± 0.0	0.0 ± 0.0	1.3 ± 0.1	1.4 ± 0.0	0.0 ± 0.0	0.4 ± 0.0
Monomer penta		0.2 ± 0.0	0.1 ± 0.0	0.0 ± 0.0	0.3 ± 0.0	0.2 ± 0.0	0.4 ± 0.0	0.3 ± 0.0
Monomer anhydro		0.0 ± 0.0	0.3 ± 0.0	0.4 ± 0.0	0.0 ± 0.0	0.0 ± 0.0	0.0 ± 0.0	0.6 ± 0.0
Dimers (Total)		50.3 ± 0.0	44.9 ± 0.0	43.9 ± 0.6	57.9 ± 1.6	53.6 ± 0.0	50.4 ± 0.0	46.8 ± 0.0
Dimers (DD)		42.1 ± 0.1	44.4 ± 0.1	43.4 ± 0.8	47.2 ± 0.9	46.6 ± 0.1	50.1 ± 0.0	46.1 ± 0.0
Dimers (LD)		8.2 ± 0.1	0.5 ± 0.0	0.5 ± 0.0	10.7 ± 0.1	7.0 ± 0.1	0.3 ± 0.0	0.7 ± 0.0
Dimers anhydro		3.9 ± 0.0	4.3 ± 0.2	3.9 ± 0.0	6.3 ± 2.7	5.3 ± 0.1	6.7 ± 0.0	7.4 ± 0.0
Trimers (Total)		21.8 ± 0.0	21.7 ± 0.0	23.7 ± 0.1	16.0 ± 1.6	19.3 ± 0.8	12.9 ± 0.0	17.1 ± 0.0
Trimer anhydro		1.6 ± 0.0	3.5 ± 0.0	3.5 ± 0.0	1.6 ± 0.0	2.5 ± 0.0	3.0 ± 0.0	5.5 ± 0.0
Tetramers (Total)		3.9 ± 0.0	6.0 ± 0.0	7.4 ± 0.2	1.2 ± 0.0	2.6 ± 0.0	1.4 ± 0.0	3.2 ± 0.0
Tetramers (anhydro)		0.6 ± 0.0	1.3 ± 0.0	1.5 ± 0.0	0.0 ± 0.0	0.6 ± 0.0	0.5 ± 0.0	1.5 ± 0.0
Dipeptides (Total)		0.0 ± 0.0	0.0 ± 0.0	0.0 ± 0.0	0.0 ± 0.0	0.0 ± 0.0	0.0 ± 0.0	0.3 ± 0.0
Tripeptides (Total)		7.7 ± 0.0	0.4 ± 0.0	0.2 ± 0.0	8.9 ± 0.1	6.2 ± 0.0	0.8 ± 0.0	0.4 ± 0.0
Tetrapeptides (Total)		92.0 ± 0.0	99.4 ± 0.0	99.7 ± 0.0	90.5 ± 0.0	93.6 ± 0.0	98.3 ± 0.0	98.7 ± 0.0
Pentapeptides		0.3 ± 0.0	0.3 ± 0.0	0.1 ± 0.0	0.6 ± 0.0	0.2 ± 0.0	0.8 ± 0.0	0.6 ± 0.0
3-3-cross-linkage		4.6 ± 0.0	0.3 ± 0.0	0.2 ± 0.0	5.7 ± 0.0	3.9 ± 0.0	0.2 ± 0.0	0.4 ± 0.0
4-3-cross-linkage		38.1 ± 0.0	41.2 ± 0.0	43.1 ± 0.0	34.8 ± 2.1	37.7 ± 0.7	34.7 ± 0.0	36.9 ± 0.0
Chain ends (anhydros)		2.6 ± 0.0	4.0 ± 0.0	3.9 ± 0.1	3.7 ± 0.8	3.6 ± 0.0	4.5 ± 0.0	6.5 ± 0.0
Average chain length		37.8 ± 1.6	25.3 ± 1.7	26.0 ± 2.5	28.5 ± 46.2	27.5 ± 1.3	22.4 ± 0.0	15.4 ± 0.0
Degree of cross-linkage		42.6 ± 0.0	41.5 ± 0.0	43.3 ± 0.0	40.5 ± 2.5	41.6 ± 0.5	34.9 ± 0.0	37.2 ± 0.0
% peptides in cross-links		76.0 ± 0.1	72.7 ± 0.0	75.0 ± 0.0	75.1 ± 7.1	75.5 ± 0.9	64.8 ± 0.0	67.2 ± 0.0

[a]Values are mean ± variation of two biological repeats.

970

971 **Table S2:** Strains and plasmids used in this study
972

Strain or Plasmid	Description	Reference or Source
Strains		
A. baumannii AB5075	Wild type	(1)
A. baumannii AB5075	Δ*ldtJ*	(2)
A. baumannii AB5075	Δ*mrcA*	(2)
A. baumannii AB5075	Δ*ldtJ* Δ*mrcA*	This study
A. baumannii AB5075	Δ*mrcB*	(2)
A. baumannii AB5075	Δ*ldtJ* Δ*mrcB*	This study
A. baumannii AB5075	Δ*ldtJ* Δ*mrcA*/pEV	This study
A. baumannii AB5075	Δ*ldtJ* Δ*mrcA*/pLdtJ	This study
A. baumannii AB5075	Δ*ldtJ* Δ*mrcA*/pPBP1A	This study
A. baumannii ATCC 17978	Wild type	(3)
A. baumannii ATCC 17978	Δ*ldtJ*	(4)
A. baumannii ATCC 17978	Δ*mrcA*	(5)
A. baumannii ATCC 17978	Δ*ldtJ* Δ*mrcA*	This study
A. baumannii ATCC 17978	Δ*ldtJ* Δ*mrcA*/pEV	This study
A. baumannii ATCC 17978	Δ*ldtJ* Δ*mrcA*/pLdtJ	This study
A. baumannii ATCC 17978	Δ*ldtJ* Δ*mrcA*/pPBP1A	This study
E. coli MFD DAP-	Donor strain for conjugation	(6)
E. coli DH5α	Host strain for cloning	(7)
Plasmids		
pABcre	Derived from pAT801-RA with *cre* recombinase and *arr2*, Rif^R	(8, 9)
pJMP3665HygR	Replicative plasmid pJMP3665HygR, Hyg^R	(10)
pJMP3665HygR*::mrcA*	Replicative plasmid pJMP3665HygR, Hyg^R carrying AB5075 *mrcA* (*ABUW_0289*)	This study

pJMP3665HygR*::ldtJ*	Replicative plasmid pJMP3665HygR, Hyg^R carrying AB5075 *ldtJ* (*ABUW_1189*)	This study
pAT03	pMMB67EH with FLP recombinase, Tet^R	(11)
pAT04	pMMB67EH with REC_{Ab} system, Tet^R	(11)
pKD4	Kan^R	(12)
pMMB67EH	pMMB67EH with the Kan^R gene from pKD4 inserted into the PvuI site, Kan^R	(4)
pABBR	pABBR_MCS with the Tet^R gene from pKD4 replacing the *bla* gene, Tet^R	(5)
pABBR*::mrcA*	pABBR, Tet^R carrying 17978 *mrcA* (*A1S_3196-3197*)	(5)
pMMB67EH*::ldtJ*	pMMB67EH, Kan^R carrying 17978 *ldtJ* (*A1S_2371*)	(4)
pMMB67EH*::mrcA-flag*	pMMB67EH, Kan^R carrying the fusion 17978 *mrcA-flag*	This study
pMMB67EH*::ldtJ-flag*	pMMB67EH, Kan^R carrying the fusion 17978 *ldtJ-flag*	This study

973

974 **Table S3:** Primers used in this study.
975

Oligo Name	**Sequence (5' to 3')**
AB5075 Tn26 Insertion Primers	
5075 ABUW_1189 5'	GCCCAACATTTCACTTACGC
5075 ABUW_1189 3'	CAATTGCATCTTTCCAGCAA
5075 ABUW_0289 5'	GGCGTTTCGCATTAATTGTT
5075 ABUW_0289 3'	ATATCAAAAGGCCGTTGCAG
5075 ABUW_1358 5'	CAGGTTCTACGCTGTCACCA
5075 ABUW_1358 3'	AATGCGCCAATTACTCAAGC
ATCC 17978 Deletion Primers	

A1S_2371 Kan-FRT 5’	TTATATCCCTTCGCGTCTCAAATAAGCCAATATTAAATTCATAAGAATGAATGATTGGTGAGTTTATGGCCTAAAGGATCTGATTTTCCCTATTGCTTATATGAAAATTCTTAAGGTTGAATTAC**AGCGATTGTGTAGGCTGGAGCTGCTTCG**
A1S_2371 Kan-FRT 3’	TTAGTAAACCTAGGCTGGTTTTATTTTTATAATCAAAACAATAACTACATATTCCACGGGGCTATGCTAAAAAATTTAATAAAAAAGCCTGCATAAAGCAGGCTCTTTTAATTAAGAGGA**ATATCCTCCTTAGTTCCTATTCCG**
A1S_2371 confirm 5’	TACTTGCAGCATGTTACATCGGGTTTA
A1S_2371 confirm 3’	GGGTCAGATGCTGAAGCTGAATGGTTA
Complementation Primers	
5075 *ldtJ* BamHI 5'	**CGCGGATCCATG**TTTGTTCGCTCATTACTCGCTATGAG
5075 *ldtJ* XbaI 3'	**CGCTCTAGATTA**TTCTAAGAATTTAACAGTTACGCCTGAACG
5075 *mrcA* BamHI 5'	**CGCGGATCCATG**AAAAAGCTATCCAGTTTGGGCTTCG
5075 *mrcA* XbaI 3'	**CGCTCTAGATTA**TTCAATTTGATTAATCAAGTTTTCTAATTCATCTTTTTC
pJMP3665HygR confirm 5’	GCAATTAATGTGAGTTAGCGCG
pJMP3665HygR confirm 3’	CGTTCTGATTTAATCTGTATCAGGCT
Co-immunoprecipitation Primers	
17978 *ldtJ-flag* KpnI 5’	**CGCGGTACCATG**TTTGTTCGCTCATTACTCGC
17978 *ldtJ-flag* BamHI 3’	**CGCGGATCCTTATTTATCATCATCATCTTTATAATC**TTCTAAGAATTTAACAGTTACGCC
17978 *mrcA-flag* KpnI 5’	**CGCGGTACCATG**AAAAAGCTATCCAGTTTGGGCTTCGTGC
17978 *mrcA-flag* BamHI 3’	**CGCGGATCCTTATTTATCATCATCATCTTTATAATC**TTCAATTTGATTAATCAAGTTTTCTAATTCATCTTTTTCAC
pMMB67EH confirm 5’	CGGTTCTGGCAAATATTCTGAAA
pMMB67EH confirm 3’	CTGCGTTCTGATTTAATCTGTAT

976

977

978 **Supplementary References**

979 1. Jacobs AC, Thompson MG, Black CC, Kessler JL, Clark LP, McQueary CN, et al. AB5075, a
980 highly virulent isolate of *Acinetobacter baumannii*, as a model strain for the evaluation of
981 pathogenesis and antimicrobial treatments. mBio. 2014; 5:e01076-14.

982 2. Gallagher LA, Ramage E, Weiss EJ, Radey M, Hayden HS, Held KG, et al. Resources for
983 genetic and genomic analysis of emerging pathogen *Acinetobacter baumannii*. J Bacteriol.
984 2015; 197(12):2027–35.

985 3. Baumann P, Doudoroff M, Stanier RY. A Study of the *Moraxella* Group II. Oxidative-negative
986 Species (Genus *Acinetobacter*). J Bacteriol. 1968; 95(5):1520–41.

987 4. Kang KN, Kazi MI, Biboy J, Gray J, Bovermann H, Ausman J, et al. Septal class A penicillin-
988 binding protein activity and LD-transpeptidases mediate selection of colistin-resistant
989 lipooligosaccharide-deficient *Acinetobacter baumannii*. mBio. 2021; 12(1):e02185-20

990 5. Boll JM, Crofts AA, Peters K, Cattoir V, Vollmer W, Davies BW, et al. A penicillin-binding
991 protein inhibits selection of colistin-resistant, lipooligosaccharide-deficient *Acinetobacter*
992 *baumannii*. Proc Natl Acad Sci U S A. 2016; 113(41):E6228–37.

993 6. Kazi MI, Schargel RD, Boll JM. Generating transposon insertion libraries in Gram-negative
994 bacteria for high-throughput sequencing. J Vis Exp. 2020; (161):10.3791/61612.

995 7. Hanahan D. Studies on transformation of *Escherichia coli* with plasmids. J Mol Biol. 1983;
996 166(4):557–80.

997 8. Héritier C, Poirel L, Lambert T, Nordmann P. Contribution of acquired carbapenem-
998 hydrolyzing oxacillinases to carbapenem resistance in *Acinetobacter baumannii*. Antimicrob
999 Agents Chemother. 2005; 49(8):3198–202.

1000 9. Jacobs AC, Thompson MG, Gebhardt M, Corey BW, Yildirim S, Shuman HA, et al. Genetic
1001 manipulation of *Acinetobacter baumannii*. Curr Protoc Microbiol. 2014; 35:6G.2.1-11.

1002 10. Bacon EE, Tran JS, Nadig N, Peters JM. Modular, inducible, and titratable expression systems
1003 for *Escherichia coli* and *Acinetobacter baumannii*. Microbiol Spectr. 2024; 12(11):e0130624.

1004 11. Tucker AT, Nowicki EM, Boll JM, Knauf GA, Burdis NC, Trent MS, et al. Defining gene-
1005 phenotype relationships in *Acinetobacter baumannii* through one-step chromosomal gene
1006 inactivation. mBio. 2014; 5(4):e01313-14.

1007 12. Datsenko KA, Wanner BL. One-step inactivation of chromosomal genes in *Escherichia coli*
1008 K-12 using PCR products. Proc Natl Acad Sci USA. 2000; 97(12):6640–5.